

Validation Test Case Suite for compressible hydrodynamics computation

Raphaël Loubère

Theoretical Division, T-7, Los Alamos National Laboratory
MS-B284, Los Alamos, NM, 87545, USA
loubere@lanl.gov

September 17, 2005

Contents

1	Introduction	2
2	Context and Notation	2
3	Test Suite	2
3.1	Sod shock tube	2
3.2	Le Blanc shock tube	3
3.3	Collela-Woodward blastwave	3
3.4	Sedov problem	4
3.5	Kidder isentropic compression	5
3.6	Saltzman piston	5
3.7	Noh problem	5
3.8	Guderley on/off axes problem	5
3.9	Dukowicz problem	5
3.10	Triple point problem	5
3.11	Bubble/shock interaction	5
3.12	Rayleigh-Taylor instability	5
3.13	2D Riemann problems	10
3.14	Shaped charge	10
3.15	Double blastwave	10
4	Validation tests	10
5	Rezone component	18
6	Validation tests	18
7	Remap component	21
8	Validation tests	21
8.1	Pure remapping context	21
8.2	Simplified hydrodynamics context	24
9	Cylindrical geometry	25
10	ALE INC(ubator)	25

1 Introduction

This paper gathers several validation test cases for compressible hydrodynamics computation. This list has been developed in order to test and validate ALE INC(ubator) the 2D Arbitrary-Lagrangian-Eulerian (ALE) code on general polygons from T7 group in Los Alamos. This code deals with any type of meshes and is able to run in pure Lagrangian, Eulerian (as Lagrange plus Remap) or ALE regimes with a numerous boundary conditions available (wall, piston, pressure, periodic, etc.) allowing a wide variety in the choice of validation test cases. The flexibility of the code to handle such *scenarii* implicitly generated the need for such a list of hydrodynamics test case suite.

The rest of the paper stands as follows: first, we briefly presents the context of testing and the notation. In a second section we describe the test cases and in a third section the numerical results obtained with ALE INC. are presented.

The point of the paper is not to test the code *per se* but rather to give a list of classical test cases we used to validate the implementation of this ALE code.

2 Context and Notation

In this paper we use several sigle to shorten the notation that we describe in this section. The context of any 2D test case can be described by giving some information on:

Geometry: The geometry is the reference in which the equations are written and solved by the code. It can be Cartesian or cylindrical r-z. The key words/sigles used are Cart. for Cartesian, AWD for cylindrical with Area-Weighted Differences or CVD for cylindrical Control Volume Differences.

Scheme: The regime of the code is either L (Lagrangian), E (Lagrange+Remap), A (ALE). Moreover the ALE regime needs two more integers: K to describe which number of Lagrangian steps are performed before k Rezone and Remap step(s) is(are) done. Then any ALE regime has a key word that looks like: ALE- $K \times k$.

A Courant-Friedrichs-Lewy (CFL) condition to limit the time step during the simulation must be given, as well as the ratio of specific heat γ for the Equation of State (EOS).

Meshes: As earlier pointed out, the mesh can be of any type; structured-unstructured, triangular, polygonal, conform/unconform, etc. Therefore we introduced several sigles to describe any of these situations: P (Polygonal), S (Square 1:1 ratio), Rx (Rectangle 1:x ratio), T (Triangle), A (Adapted to the geometry, Tri+Quad), M (mass-matching square).

Initial state: The initial state is simply the exhaustive list the initial value of the thermodynamical variables (density, velocity, energy, pressure, etc.) and the conditions at the boundaries of the domain Ω , namely the Boundary Conditions (BC). Moreover a final physical time must be given.

3 Test Suite

Each test case has been chosen to test a specific property of the code: preservation of 1D symmetry, robustness, accuracy of the code, mesh adaptation, predictive capability, high deformation simulation, etc.

3.1 Sod shock tube

The Sod shock tube is a simple 1D Riemann problem.

- Domain: $\Omega = [0; 1] \times [0; 0.1]$, interface at $X = 0.5$,

- Geometry: C,
- BC: walls (left/right/top/bottom),
- Mesh: S 1:1 (square 1:1 ratio *i.e.* 101×11 nodes),
- Scheme: L, E, ALE- 10×1 ,
- EOS: $\gamma = 1.4$,
- CFL: $1/4$,
- Final Time: $t = 0.2$,
- Testing Goals: Sanity check, 1D symmetry preservation, exact solution.

Regime	Left	Right
ρ	1.0	0.125
u	0.0	0.0
p	1.0	0.1

3.2 Le Blanc shock tube

The Le blanc shock tube is a simple 1D Riemann problem.

- Domain: $\Omega = [0; 9] \times [0; y_{max}]$, interface at $X = 2.0$,
- Geometry: C,
- BC: walls (left/right/top/bottom),
- Mesh: S 1:1 (square 1:1 ratio *i.e.* $361, 721, 1441 \times 3$ nodes), M (mass-matching),
- Scheme: L, E, ALE- 10×1 ,
- EOS: $\gamma = 5/3$,
- Final Time: $t = 6.0$,
- CFL: $1/4$,
- Testing Goals: Sanity check, 1D symmetry preservation, robustness, accuracy, mass-matching mesh, exact solution.

Regime	Left	Right
ρ	1.0	0.001
u	0.0	0.0
ε	0.1	10^{-7}

3.3 Collela-Woodward blastwave

The Collela-Woodward blastwave is the interaction of two Riemann problems.

- Domain: $\Omega = [0; 1] \times [0; y_{max}]$, interfaces at $X = 0.1, X = 0.9$,
- Geometry: C,
- BC: walls (left/right/top/bottom),
- Mesh: S 1:1 (square 1:1 ratio *i.e.* $361, 601, 1201 \times 3$ nodes),
- Scheme: L, E, ALE- 10×1 ,

- EOS: $\gamma = 1.4$,
- Final Time: $t = 0.038$,
- CFL: $1/4$,
- Testing Goals: 1D symmetry preservation, robustness, accuracy, reference solution.

Regime	Left	middle	Right
ρ	1.0	1.0	1.0
u	0.0	0.0	0.0
p	1000.0	0.01	100.0

3.4 Sedov problem

The Sedov blast wave problem, [?], describes the evolution of a blast wave in a point symmetric explosion; it is an example of a diverging shock wave.

- Domain: $\Omega = [0; 1.2] \times [0; 1.2]$ or $\Omega = [0; 1] \times [0; 1]$ (for P, A meshes),
- Geometry: C, AWD,
- BC: walls,
- Mesh: S 1:1 (square 1:1 ratio *i.e* 31×31 nodes), P,
- Scheme: L, E, ALE- 10×1 ,
- EOS: $\gamma = 1.4$,
- Final Time: $t = 1.0$,
- CFL: $1/4$,
- Testing Goals: wall heating, cylindrical symmetry, spherical symmetry, accuracy, exact solution.

Regime	Left	Right
ρ	1.0	1.0
u	0.0	0.0
p	0.0	0.0

The total energy of the explosion is concentrated at the origin and has magnitude $E_{total} = 0.244816$. At time $t = 1.0$ the exact solution is a cylindrically symmetric diverging shock whose front is at radius, $r = \sqrt{x^2 + y^2} = 1$ and has a peak density of 6.0 (the solid line in Fig. 2). In our numerical experiments E_{total} is concentrated in one cell located at the origin (that is, containing the vertex $(x, y) = (0, 0)$). The specific internal energy of this cell, c is defined as $\varepsilon(c) = E_{total}/V(c)$, where $V(c)$ is the volume of the cell. Therefore the initial pressure in this cell is $p = (\gamma - 1)\rho\varepsilon = 0.4E_{total}/V(c)$.

Polygonal Mesh constructor:

The computational domain is one quarter of a circular disk with radius of $r_{max} = 1.2$. A polygonal mesh is constructed in the computational domain using a Voronoi diagrams (see, for example, [?]) for the set of point defined as follows:

$$x_{i,j} = r_j \sin(\theta_{i,j}) \quad y_{i,j} = r_j \cos(\theta_{i,j}); \quad j = 1, \dots, J; \quad i = 1, \dots, I(j).$$

where

$$r_j = r_{max} \cdot \frac{j-1}{J}, \quad I(j) = \mathbf{round}((j-1) \frac{\pi}{2}), \quad \theta_{i,j} = \frac{i-1}{I(j)} \cdot \frac{\pi}{2}, \quad J = 31.$$

and function $\mathbf{round}(x)$ returns the closest integer to x . According to these formulas, on each circle of radius r_j points are distributed so that the distance between adjacent points along the circle is approximately equal to $\Delta r = r_{max}/(J-1)$. The total number of points is 775. There is exactly one Voronoi cell corresponding to each point. The mesh consists of a mixture of convex polygons: quadrilaterals, pentagons and hexagons, and the total number of vertices is 1325; the mesh is shown in Fig. 3 (top-left panel). The resulting polygonal mesh has approximately the same resolution as the quadrilateral mesh presented in Fig. 1.

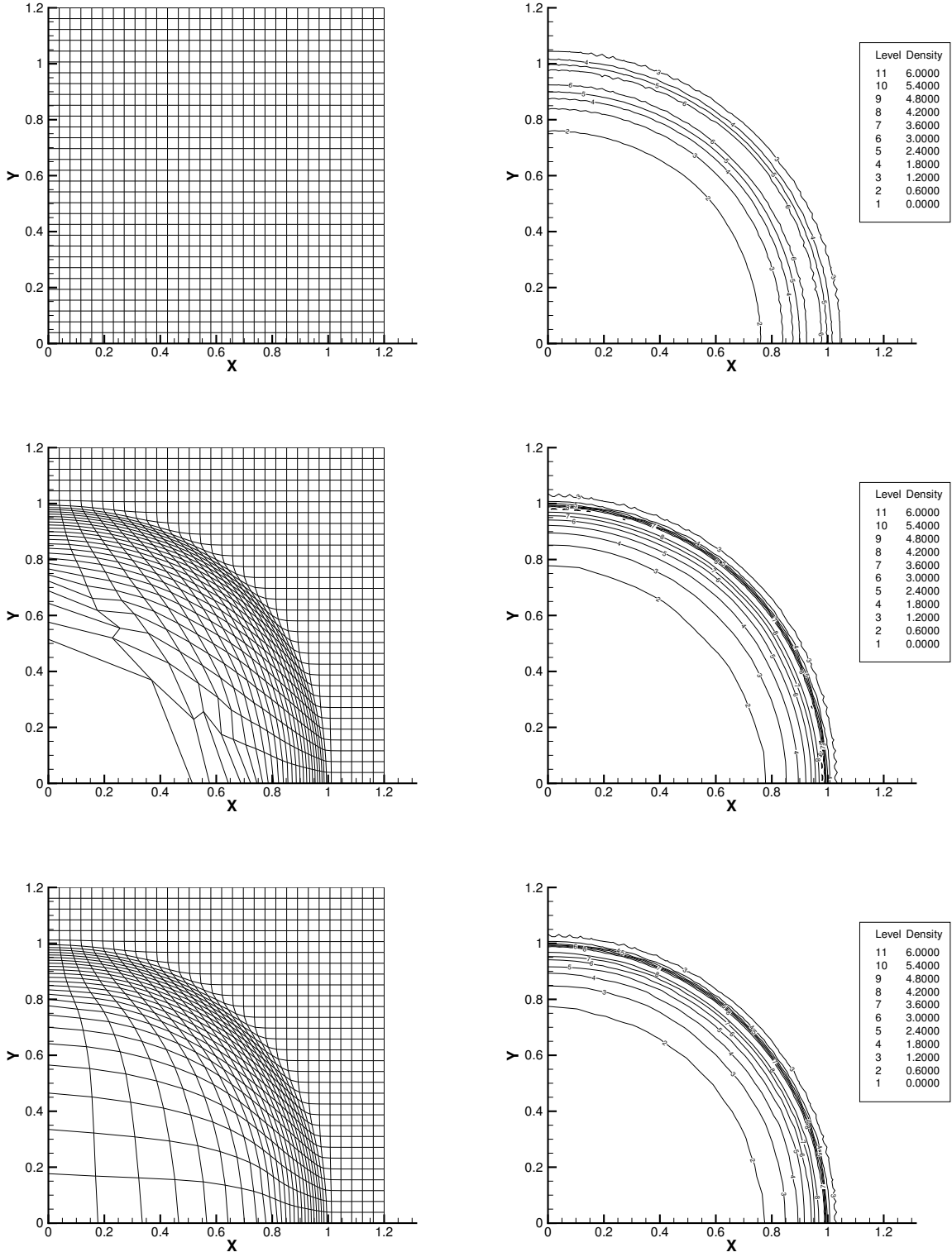


Figure 1: Sedov problem — Quadrilateral Mesh. Mesh (left), and density isolines (right) at $t = 1.0$ — Eulerian regime (top), Lagrangian regime (middle), ALE regime (bottom).

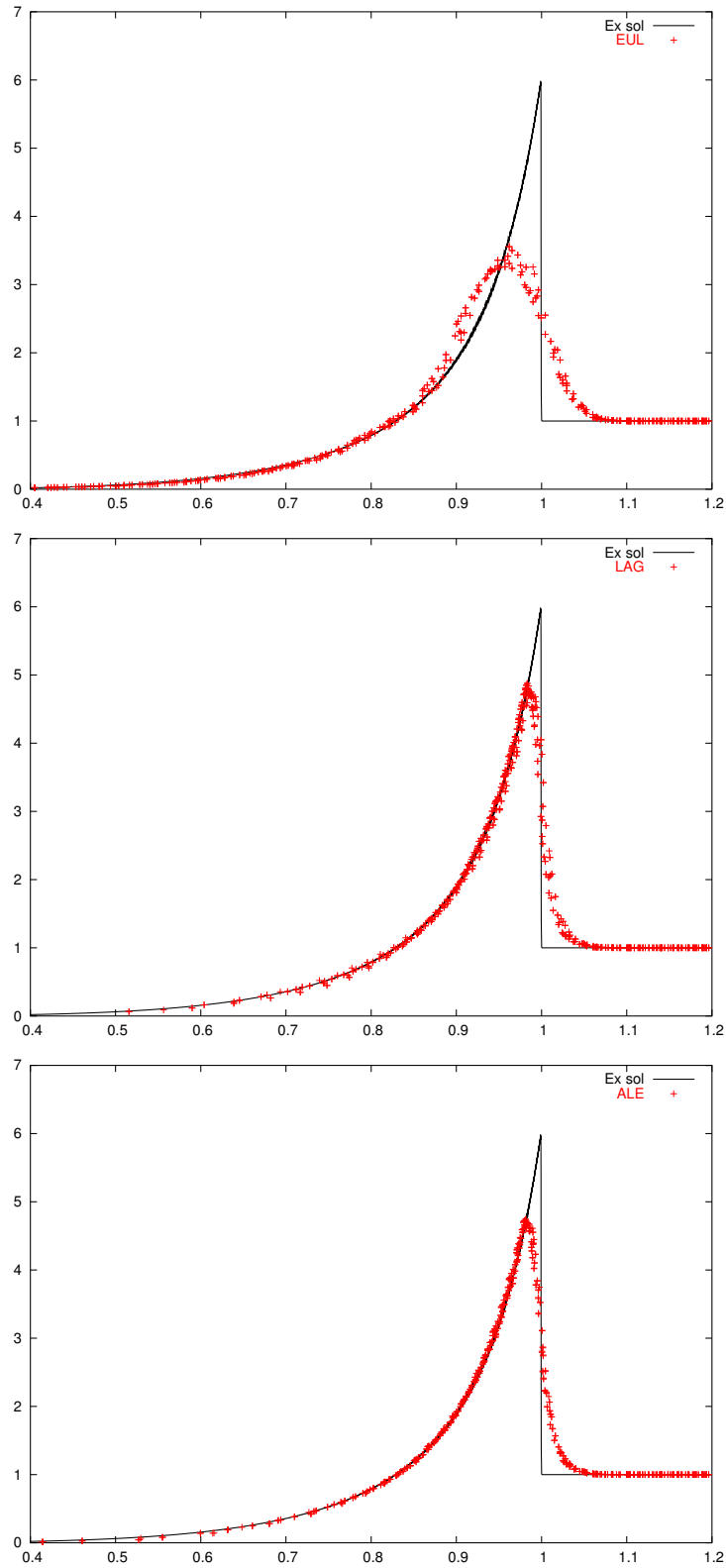


Figure 2: Sedov problem — Quadrilateral Mesh. Density at $t = 1.0$ as a function of the radius (solid line exact solution) — Eulerian regime (top), Lagrangian regime (middle), ALE regime (bottom).

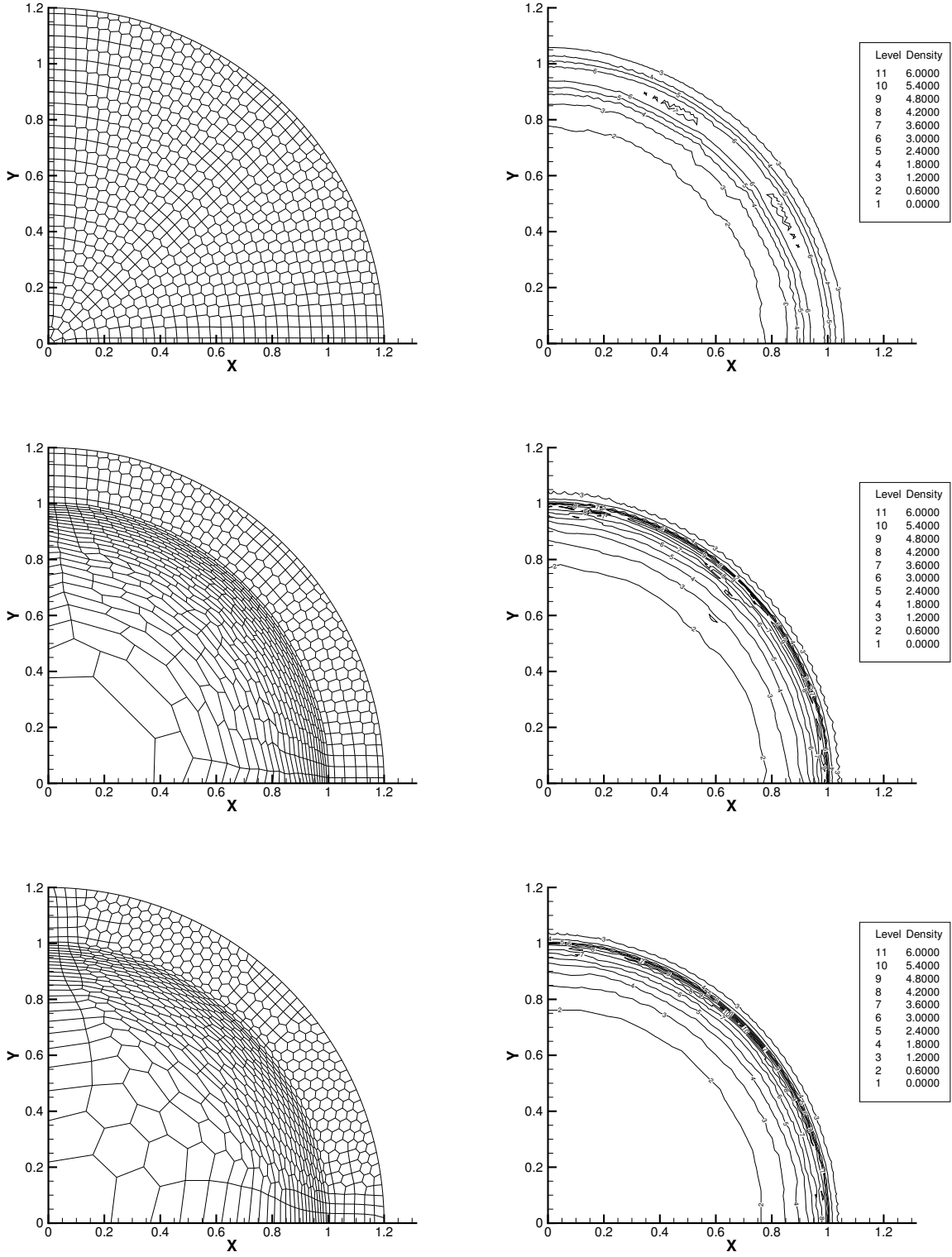


Figure 3: Sedov problem — Polygonal Mesh. Mesh (left), and density isolines (right) at $t = 1.0$ — Eulerian regime (top), Lagrangian regime (middle), ALE regime (bottom).

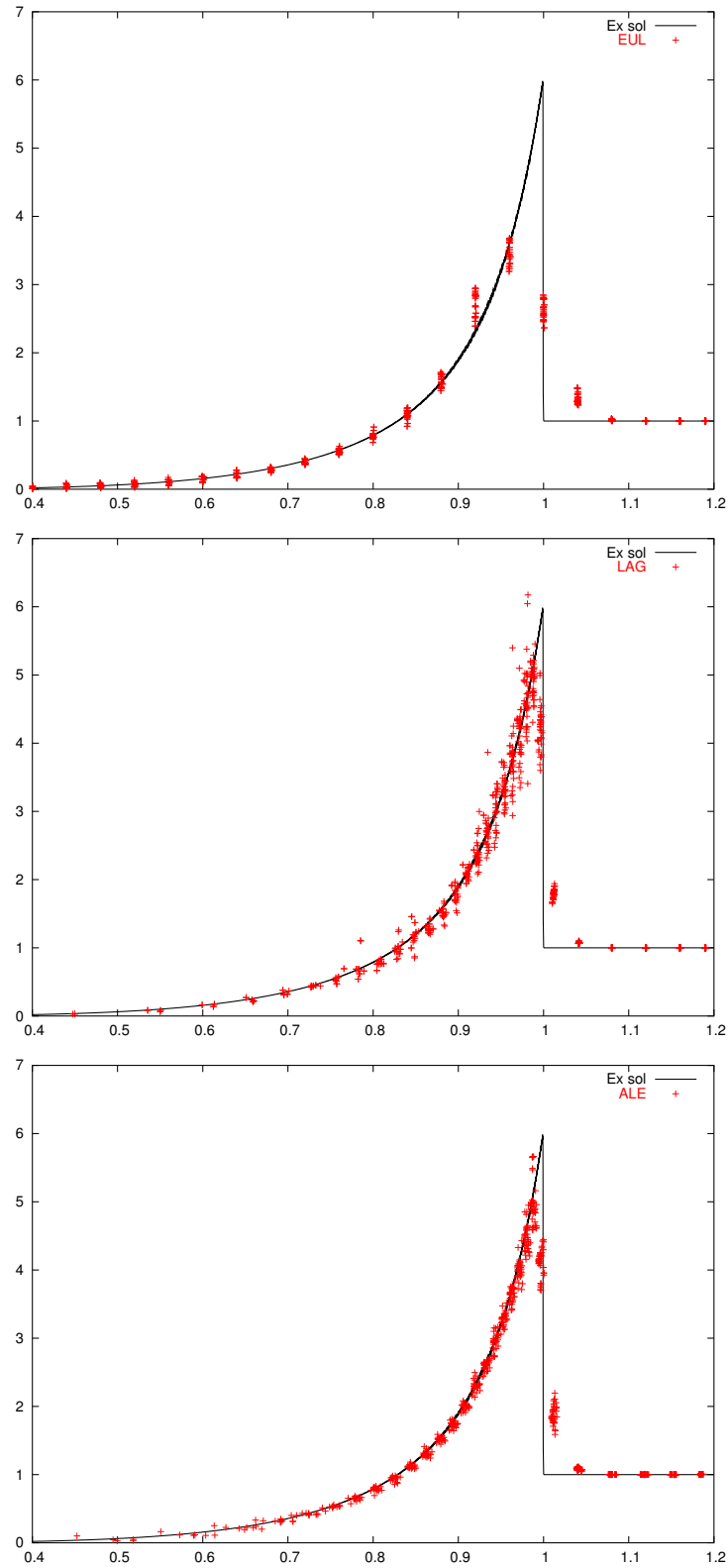


Figure 4: Sedov problem — Polygonal Mesh. Density at $t = 1.0$ as a function of the radius (solid line exact solution) — Eulerian regime (top), Lagrangian regime (middle), ALE regime (bottom).

3.5 Kidder isentropic compression

Regime	Mesh	Purpose
L	S	sanity of L, ex sol
L	T, X2, X4	sanity of L, ex sol
L	P	sanity of L, ex sol
ALE	P	sanity of ALE

3.6 Saltzman piston

Regime	Mesh	Purpose
L	S	robustness
L	Rx	robustness
ALE	S,Rx	mesh adapt. (rezone)

3.7 Noh problem

Regime	Mesh	Purpose
L (Cart)	S,P	wall heating, cylind. symmetry, accuracy
L (AWD)	S,P	wall heating, spher. symmetry, accuracy
ALE	S,P	mesh adapt.

3.8 Guderley on/off axes problem

Regime	Mesh	Purpose
L	S (on/off)	robustness
ALE	S (on/off)	mesh adapt. (especially off)

3.9 Dukowicz problem

Regime	Mesh	Purpose
L	A, P	interact. of waves, reflect., refract., predictive capab.
ALE	A, P	interact. of waves, reflect., refract., predictive capab.

3.10 Triple point problem

Regime	Mesh	Purpose
L???	S, A	predictive capab., vorticity simulation, interf. preserv.
ALE	S, A	predictive capab., vorticity simulation, interf. preserv., mesh smoothing

3.11 Bubble/shock interaction

Regime	Mesh	Purpose
L	A,P	experimental data reproduction with accuracy
ALE	A,P	experimental data reproduction with accuracy

3.12 Rayleigh-Taylor instability

Regime	Mesh	Purpose
ALE	R	quasi incompressible limit, vorticity, robustness, high deformation

3.13 2D Riemann problems

Regime	Mesh	Purpose
ALE	S	Comp. wt other codes, mesh smoothing
E	S	Comp. wt other codes

3.14 Shaped charge

Regime	Mesh	Purpose
ALE	A	high deformation, mesh smoothing, interface preserv.

3.15 Double blastwave

Regime	Mesh	Purpose
ALE	A	high deformation, mesh smoothing, wave interactions

4 Validation tests

The validation has been performed mostly by running as many test cases as possible. These test cases have been run in 1D/2D, with one or several EOS, in Cartesian/cylindrical geometry, on quadrangular mesh/polar mesh/polygonal mesh. . . Moreover these tests have been chosen such as they have either an exact solution or a known reference solution (computed on a very refined mesh). For example the component has been tested on this non exhaustive list:

- Riemann problems (Sod, Le Blanc. . .),
- Piston problems (straight piston, Saltzman. . .),
- Collela-Woodward blastwave,
- Noh/Guderley/Sedov problem,
- . . .

Several of the results given by the Lagrangian component can be found in [8], [10], [12]. We will present a set of results given by the Lagrangian scheme. This section is not devoted to make a behavior study of the Lagrangian scheme but rather to show the ability of the scheme on classical problems. Therefore we do not extensively comment the results.

All the results have been produced using the tensor artificial viscosity.

1D Sod Riemann problem. The Sod problem is a Riemann shock tube with a relatively small discontinuity, and so is a very mild test. Its solution consists of a left rarefaction, a contact discontinuity and a right shock and the exact solution is illustrated in Fig. 5 by the solid line. In our numerical experiments, the computational domain is $1 \geq x \geq 0$. The discontinuity is initially at 0.5. The domain is filled with an ideal gas with $\gamma = 1.4$. The density/pressure values on the left side of the discontinuity are 1.0/1.0, while those on the right side are 0.125/0.1. In Figure 5, we present numerical results for the density, specific internal energy and velocity at the final time $t = 0.25$ for a run with an initial 301×5 quadrangular mesh computational cells.

1D LeBlanc Shock Tube Problem. In this extreme shock tube problem the initial discontinuity separates a region of very high energy and density from one of low energy and density. This is a much more severe test than the Sod Problem. The computational domain is $9 \geq x \geq 0$ and is filled with an ideal gas with $\gamma = 5/3$. The gas is initially at rest. The initial discontinuity is at $x = 0.3$: $(\rho, \varepsilon) = (1., 0.1)$ for $x < 3.$ and $(0.001, 10^{-7})$ for $x > 3.$. The solution consists of a rarefaction moving to the left, and a contact discontinuity and a strong shock moving to the right — solid line in Fig 6. At the final time of $t = 6.0$, the shock wave is located at $x = 7.975$ and the Lagrangian scheme gives the results in Fig.6 for the density, specific internal energy and velocity.

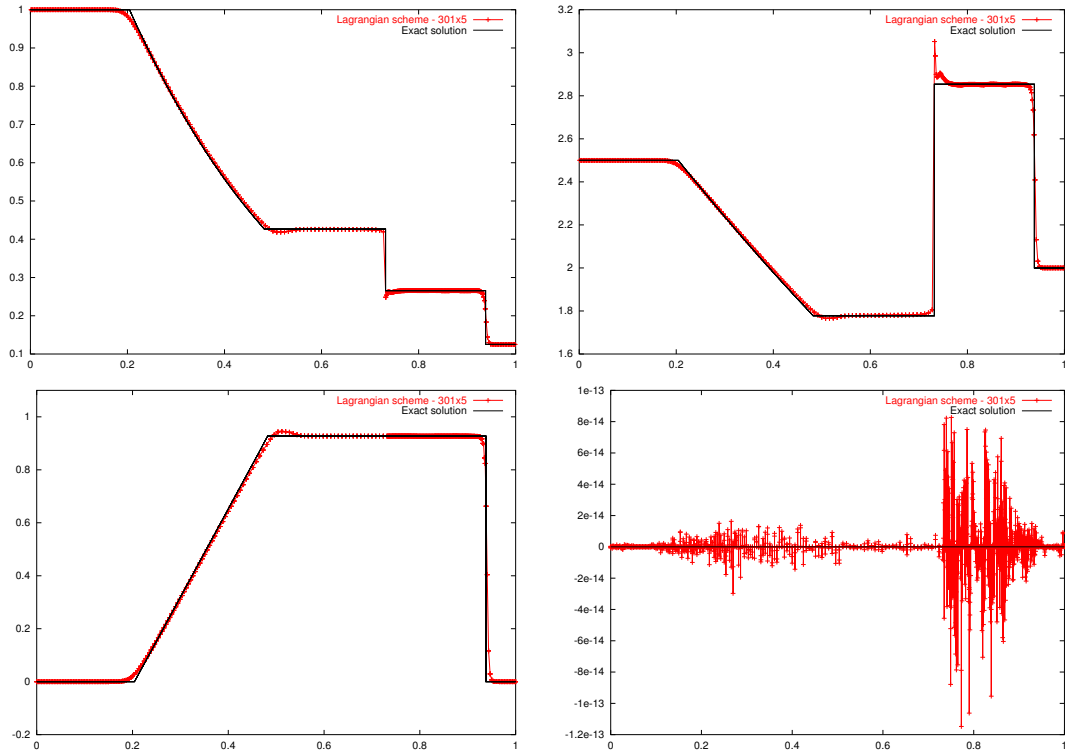


Figure 5: Sod Riemann problem at $t = 0.25$ — Lagrangian scheme results with an initial quadrangular 301×5 grid — From top-left to bottom-right: density, specific internal energy, x -component of velocity and y -component of velocity.

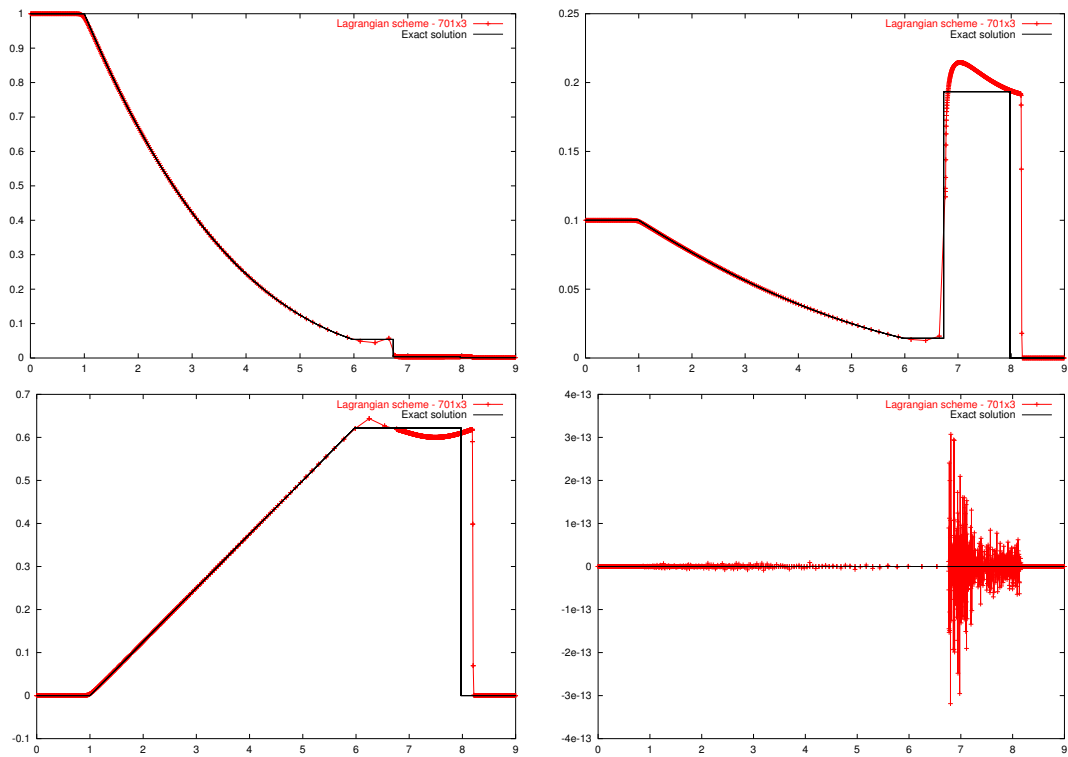


Figure 6: Le Blanc Riemann problem at $t = 6.0$ — Lagrangian scheme results with an initial quadrangular 701×3 grid — From top-left to bottom-right: density, specific internal energy, x -component of velocity and y -component of velocity.

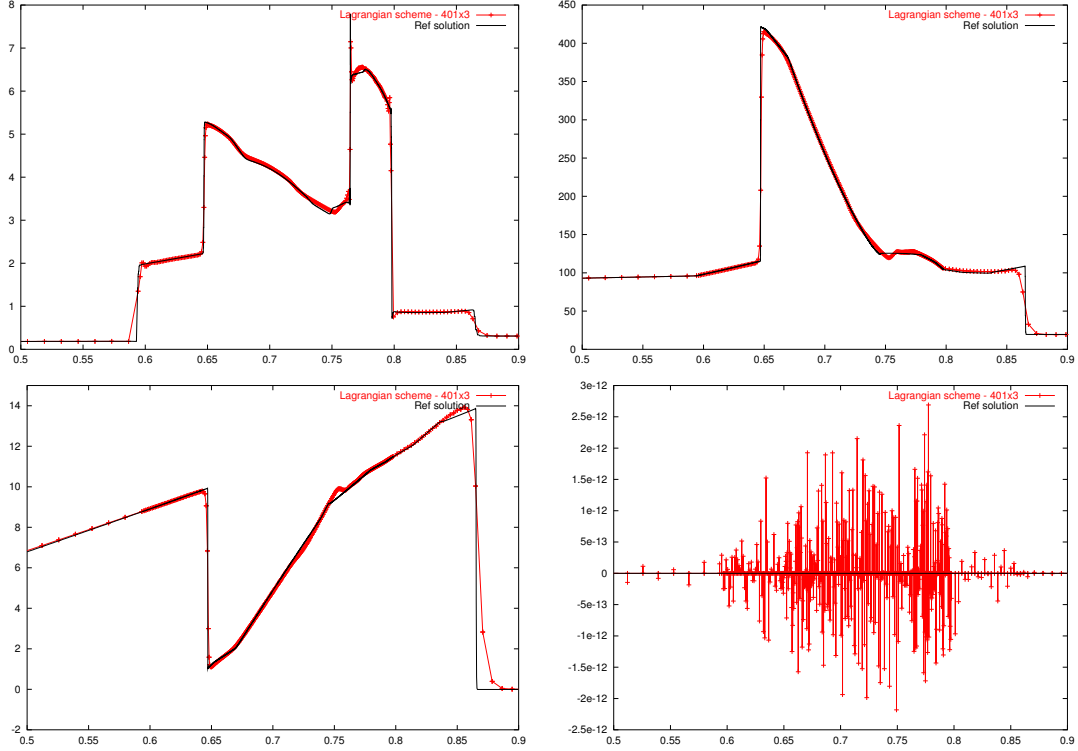


Figure 7: Collela-Woodward blastwave at $t = 0.038$ — Lagrangian scheme results with an initial quadrangular 401×3 grid — From top-left to bottom-right: density, pressure, x -component of velocity and y -component of velocity.

1D Collela-Woodward blastwave. The computational domain for this problem has length one, with reflecting walls at the both ends. The gas is an ideal gas with $\gamma = 1.4$. At $t = 0.$, the gas is at rest with an uniform density equal to 1.. The initial pressure is 1000.0 in the leftmost tenth of the domain, 100.0 in the rightmost tenth, and 0.01 everywhere else. The final problem time is $t = 0.038$. Initially, two shocks and two contacts develop at the initial discontinuities and propagate toward one another, while two rarefactions develop, propagate toward the walls, and reflect off them. As time progresses, these six initial waves interact and create additional contact discontinuities. There is no analytical solution for this problem and typically a solution obtained by purely Lagrangian method with very high resolution ($N_x = 3600$ cells in our case) is considered as the reference "truth" (the solid line in Fig. 7). In Fig.7 are presented the density, pressure and velocity for an initial 401×3 quadrangular grid.

2D Noh problem (Cartesian). In a quarter of the unit disk a gas ($\gamma = 5/3$) is initiated with $\rho_0 = 1$, $\varepsilon_0 = 0$ and $\mathbf{u}(x, y) = (-x/\sqrt{x^2 + y^2}, -y/\sqrt{x^2 + y^2})$. A shock wave is generated at the origin and diverges as presented in Fig.8 at $t = 0.6$. The exact solution at position r and time t is given by the following relations, in which d identifies the geometry of the problem (1 for 1D Cartesian, 2 for 1D cylindrical, 3 for 1D spherical), ρ_0 is the uniform initial density, and u_0 is the uniform velocity ($u_0 = \|\mathbf{u}\| = 1$):

$$\{\rho, \varepsilon, u\} = \begin{cases} \left\{ \rho_0 \left(\frac{\gamma+1}{\gamma-1} \right)^d, \frac{1}{2} u_0^2, 0 \right\} & \text{if } r < r_s, \\ \left\{ \rho_0 (1 - (u_0 t/r))^d, 0, u_0 \right\} & \text{if } r > r_s, \end{cases} \quad (4.1)$$

where the position of the shock r_s is given by

$$r_s = U_s t \text{ with the shock speed } U_s = \frac{1}{2}(\gamma - 1)|u_0|. \quad (4.2)$$

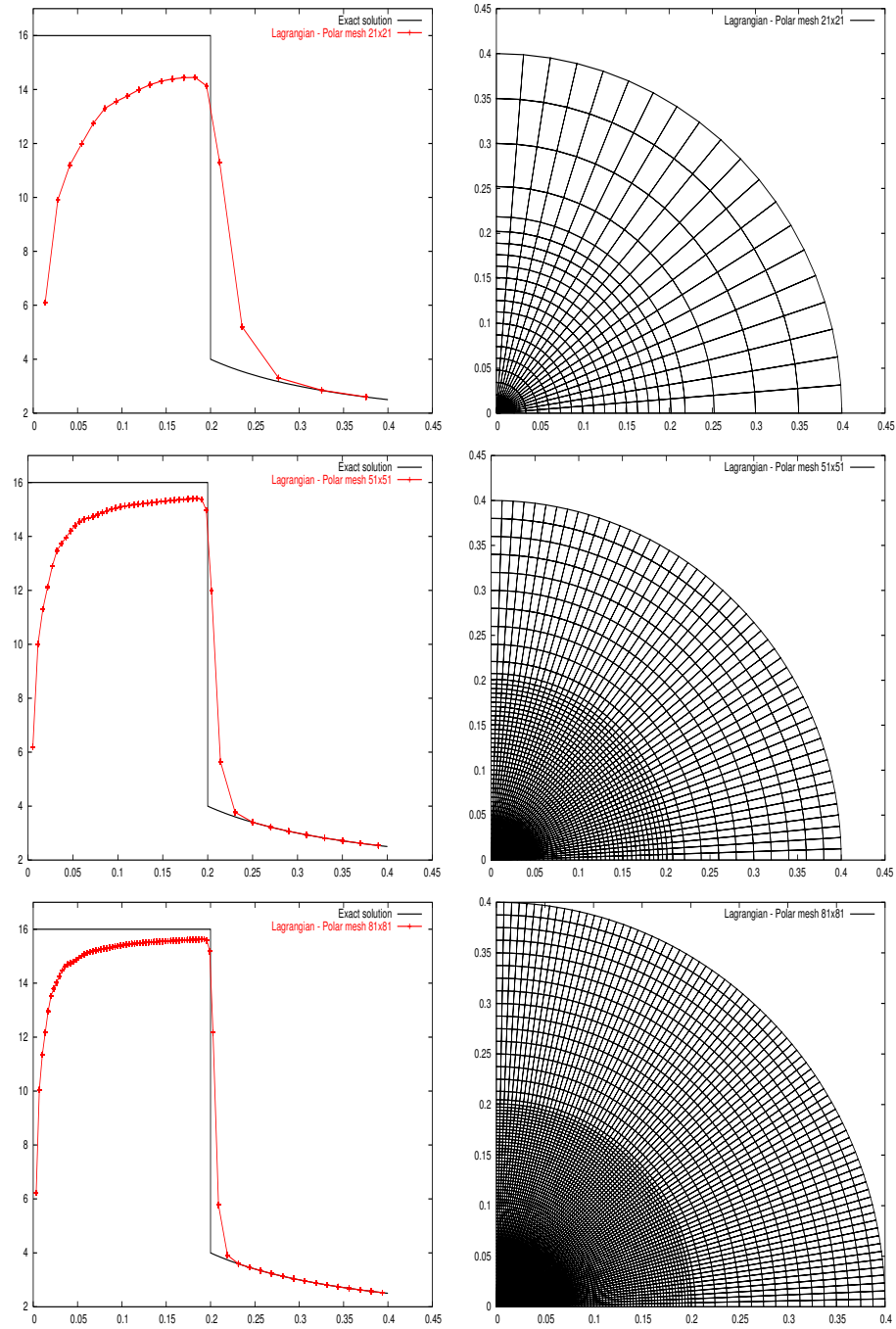


Figure 8: Noh problem at $t = 0.6$ — Lagrangian scheme results with an initial polar 21×21 (top), 51×51 (middle) and 81×81 (bottom) grids— Left: density as a function of radius — Right: final mesh.

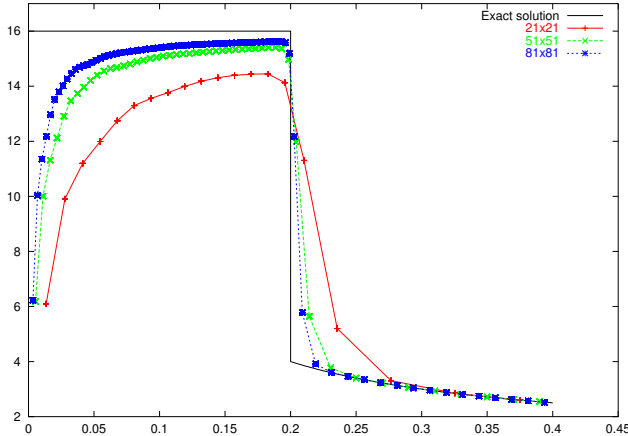


Figure 9: Noh problem at $t = 0.6$ — Lagrangian scheme results with an initial polar 21×21 , 51×51 and 81×81 grids — Density as a function of radius.

The initial mesh is a polar mesh generated with $n_x = 21, 41, 81$ points $0 \leq \theta \leq \pi/4$ on any of the $n_y = 21, 41, 81$ circles $0 \leq r \leq 1$. In this configuration the exact solution is simply given by ($r_s = 0.2$, $U_s = \frac{1}{3}$)

$$\{\rho, \varepsilon, u\} = \begin{cases} \left\{ 16, \frac{1}{2}, 0 \right\} & \text{if } r < 0.2, \\ \left\{ \left(1 + \frac{3}{5} \frac{1}{r}\right), 0, 1 \right\} & \text{if } r > 0.2, \end{cases} \quad (4.3)$$

In fig.9 is presented the density as a function of the radius for the three previous polar grids, showing the convergence of the method.

2D Guderley problem. In a quarter of the unit disk a gas ($\gamma = 5/3$) is initiated with $\rho = 1$, $\varepsilon = 0$ and $\mathbf{u} = (0, 0)$. The velocity boundary condition for the points on the external circle being for all time step t_n :

$$\mathbf{u}_i^{n,BC} = \left(-x_i^n / \sqrt{(x_i^n)^2 + (y_i^n)^2}, -y_i^n / \sqrt{(x_i^n)^2 + (y_i^n)^2} \right). \quad (4.4)$$

A shock wave is generated at boundary circle and converges toward the center as presented in Fig.10 at $t = 0.6$ and $t = 0.8$ (after bouncing).

The initial mesh is a polar mesh generated with 21 points $0 \leq \theta \leq \pi/4$ on any of the 21 circles $0 \leq r \leq 1$. There exists no exact solution to this problem.

2D Sedov problem. We consider the cylindrically symmetric Sedov problem, in Cartesian coordinates (x, y) . The total energy of the explosion is concentrated at the origin and has magnitude $E_{total} = 0.244816$ (similar to [9]). The material is an ideal gas with $\gamma = 1.4$ and initially is at rest. At time $t = 1.0$ the exact solution is a cylindrically symmetric diverging shock whose front is at radius, $r = \sqrt{x^2 + y^2} = 1$ and with a peak density of 6.0 (the solid line in Fig. 11). In our numerical experiments E_{total} is concentrated in one cell located at the origin (that is, containing the vertex $(x, y) = (0, 0)$). The specific internal energy of this cell, c is defined as $\varepsilon(c) = E_{total}/V(c)$. The initial meshes are either quadrilateral or polygonal.

For each simulation we show both the initial and the final mesh, with 11 density isolines equally distributed in magnitude between 0.0 and 6.0. (Fig. 11). Each isoline has a label that refers to a density value in the legend scale. Also we show a 1D plot of density as a function of the radius, r , and a corresponding plot of the exact solution. The 1D plots demonstrate how well the numerical solution preserves cylindrical symmetry.

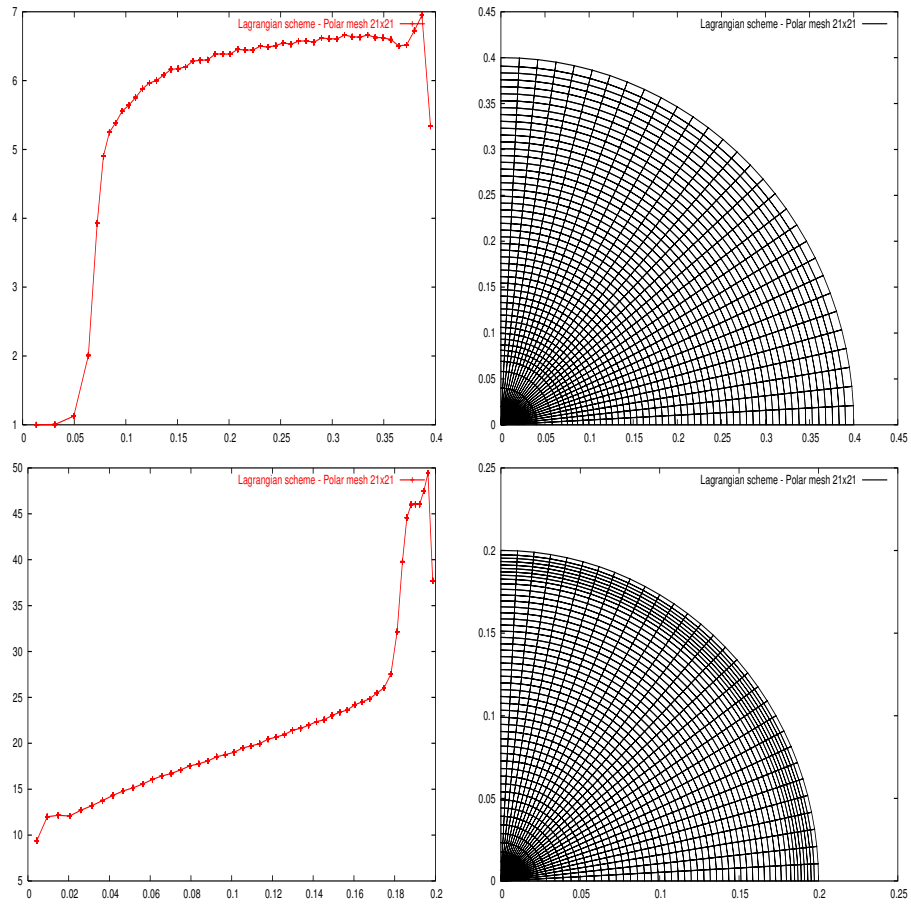


Figure 10: Guderley problem at $t = 0.6, t = 0.8$ — Lagrangian scheme results with an initial polar 21×21 grid — Left: density as a function of radius — Right: final meshes.

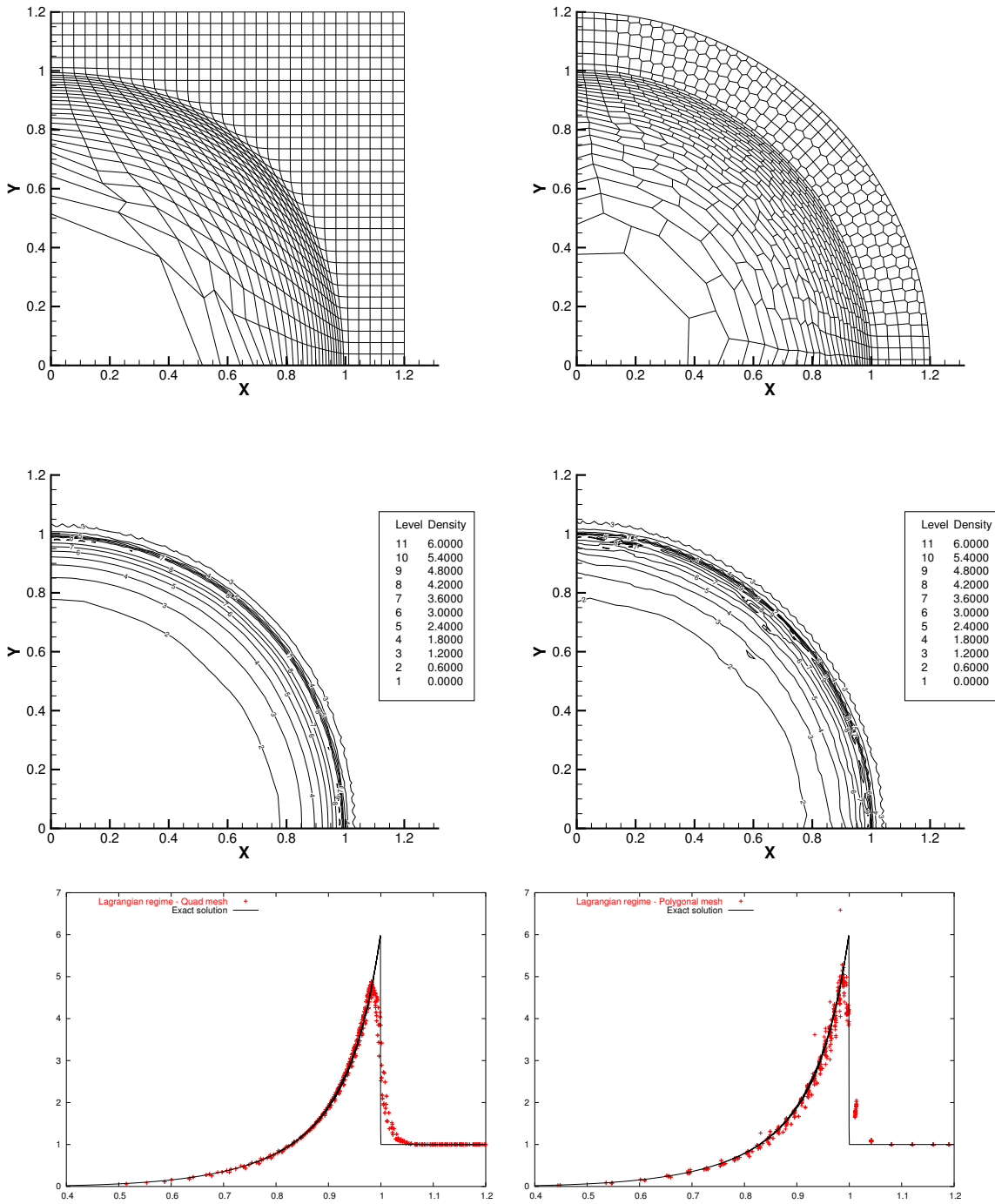


Figure 11: Sedov problem — Pure Lagrangian scheme — Meshes (top), isolines of density (middle) and density as a function of radius (bottom) at $t = 1.0$ — Left: quadrilateral mesh, Right: polygonal mesh.

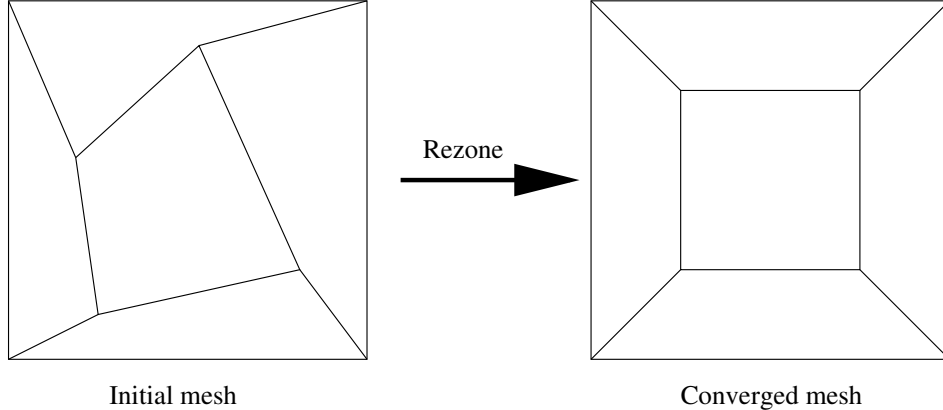


Figure 12: Example of simple verification test for the rezoning component where the calculation can be done “by hand”— Initial mesh and mesh after convergence of the rezoning process.

5 Rezone component

6 Validation tests

The tests ran to validate the rezone component are of three kinds. The first type is a simple geometrical mesh improvement when the initial mesh is small enough for us to write down every step of the optimization process and check that at the convergence point we end up with the optimal mesh (in the sense of condition number). For example in Fig.12 is an example of initial and final (converged) meshes.

In Fig.13 a 21×21 mesh made of perfect quadrilateral cells is randomly perturbed for each point i by the equation

$$\tilde{X}_i = X_i + \frac{2r_x - 1}{10}, \quad (6.1)$$

$$\tilde{Y}_i = Y_i + \frac{2r_y - 1}{10}, \quad (6.2)$$

$$(6.3)$$

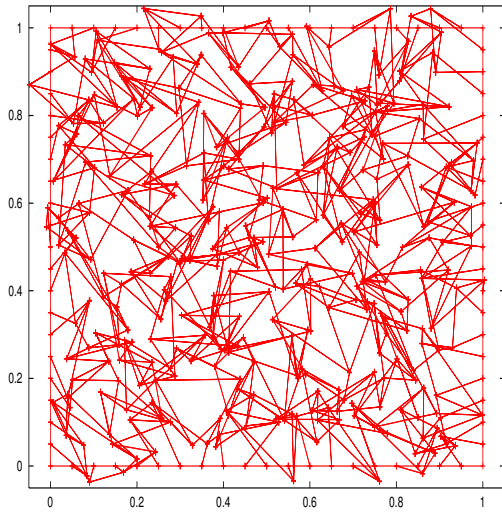
where r_x, r_y are two random numbers between 0 and 1. The initial tangled mesh is then given in Fig.13 (a). We untangle the mesh (see Fig.13 (b)) β being given by an absolute constant set to $L_{character}/100$, where $L_{character} = \frac{1}{N_c}(x_{max} - x_{min}) * (y_{max} - y_{min})$ and N_c is the number of cells. Remind that the β factor could be set to 0. The next step is to improve the mesh quality with the rezone strategy as shown in (c) and (d). The improvement converges to the perfect quadrangular mesh as expected (see Fig.13 (e)).

The second kind of validation tests is performed on bigger mesh with interfaces where we can still guess the type of evolution the mesh has to have to reach the “perfect” mesh (in the condition number sense). On this test cases we are still checking the increase of the geometrical quality during the process.

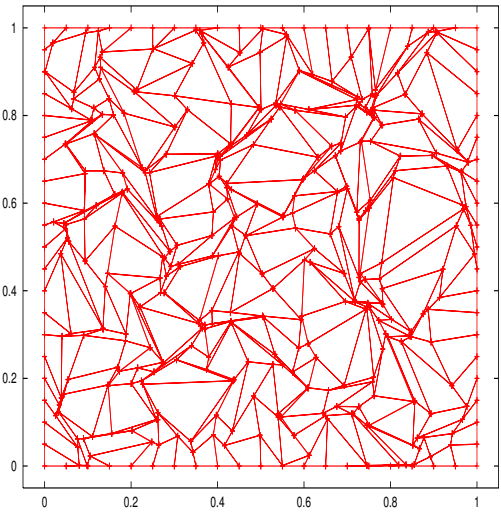
The third kind is to produce a tangled mesh with or without interfaces. Then we ask the component to untangle it, and to improve the quality. For example in Fig.14 we start with an interface from a Rayleigh-Taylor instability simulation (a), generate a mesh on the top of it (b). This interface is fixed (or frozen). Then the code successively untangle the mesh (c) and improve its quality (d).

Obviously if the interface does not exist then the convergence process would have end up to a perfect quadrilateral mesh. The validation has been performed mostly by running as many test cases as possible in ALE or Euler regimes and simply check the quality and validity of the meshes generated by the component. Some validation test results can be found in [18], [26], [27], [30].

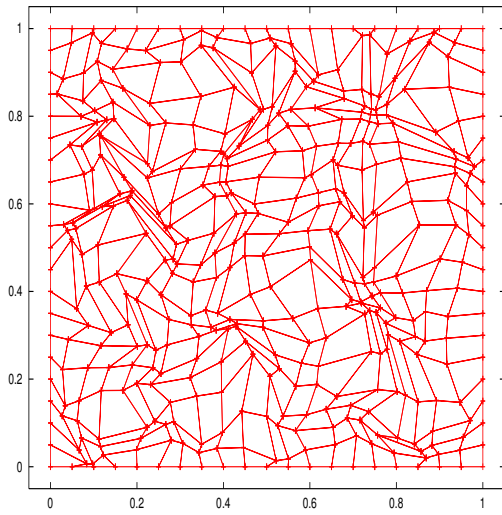
The speed-up of this component has been drastically improved by the version of V.Dyadechko which allows to use this rezoning process on big meshes with an acceptable computational time.



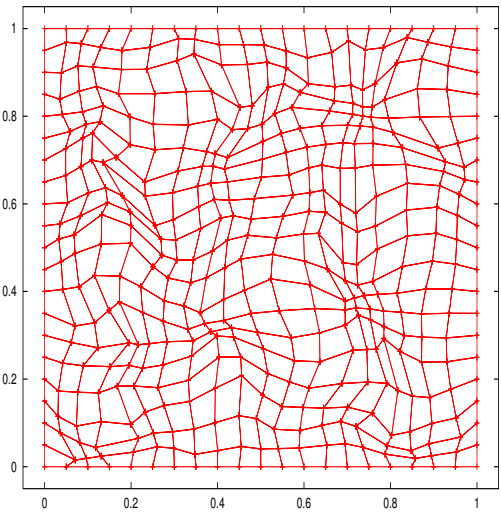
(a) Initial tangled mesh



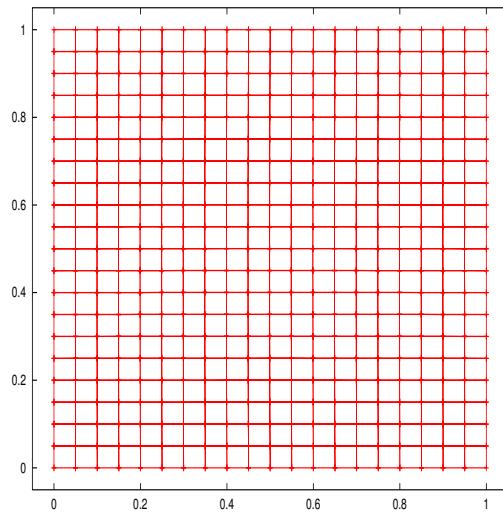
(b) Untangled mesh



(c) Mesh during the improvement

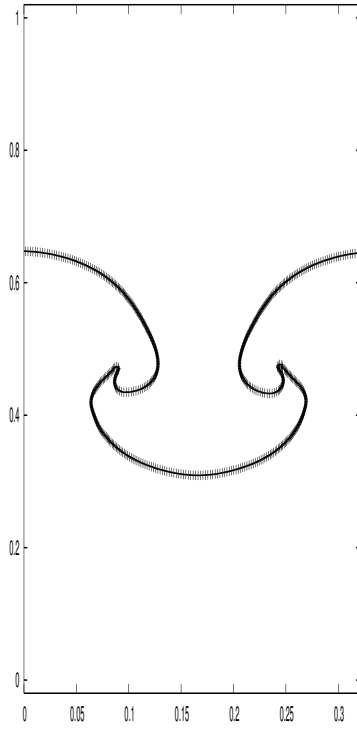


(d) Mesh during the improvement

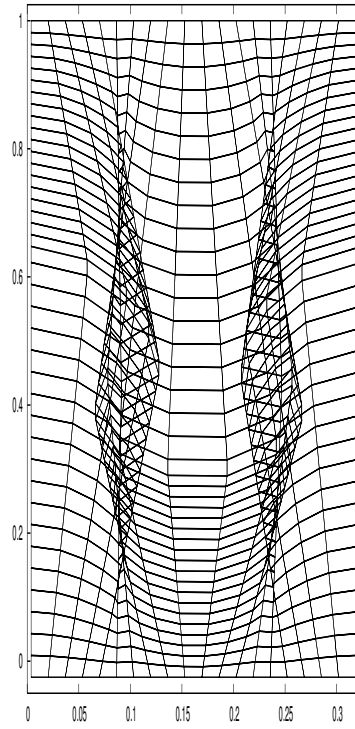


(e) Mesh after convergence of the rezoning process

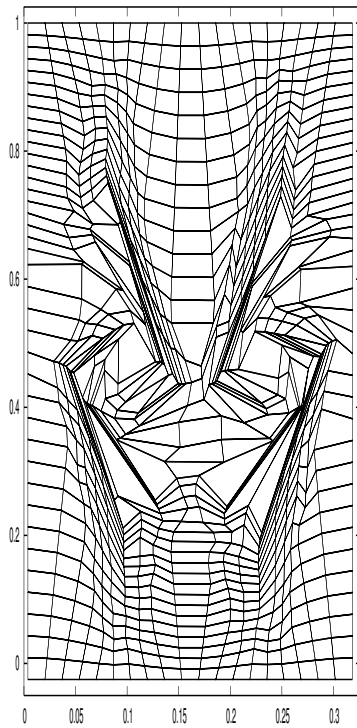
Figure 13: Verification test for the rezoning component in on a 21×21 randomly perturbed quadrangular mesh — (a) Initial tangled mesh, (b) Untangled mesh, (c,d) Mesh after two steps of improvement, (e) Mesh after convergence of the rezoning process.



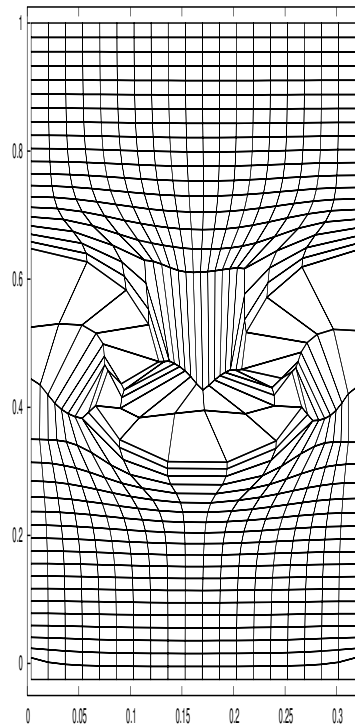
(a) Interface



(b) Initial tangled mesh



(c) Mesh after untangling process



(d) Mesh after convergence of the rezoning process

Figure 14: Verification test for the rezoning component in presence of a fixed interface crossing the domain — (a) Interface, (b) Initial tangled mesh, (c) Mesh after the untangling process, (d) Mesh after convergence of the rezoning process.

7 Remap component

8 Validation tests

In order to validate the remapping component we check it within two contexts:

- 1- a pure remapping context; no real hydrodynamics involved and an artificial rezoning process is enforced,
- 2- a simplified hydrodynamics context; 1D flow with exact solutions but treated in 2D with a simplified rezoning process — as instance a Lagrange+Remap regime of the code.

In an ALE context it is quite difficult to separate the effect of the hydrodynamics, the rezoning and the remapping. However one can check several “simple” properties like the conservation of mass, momentum and total energy, or the respect of the positivity, or the respect of a maximum principle before and after remapping. These properties are in fact requirements of the method, we do not pretend that fulfilling these requirements ensures the code to be fully validated: they are necessary conditions but not sufficient conditions!

8.1 Pure remapping context

In order to test the remapping component (independently from ALE INC.), we need to define a fluid state (profiles of density, velocity, specific internal energy) and an artificial rezoning process.

The rezone strategy used in this section is called the tensor product grid rezoning. This process starts from an initial 2D quadrangular grids ($\Omega = [0, 1] \times [0, 1]$, $n_x \times n_y$ nodes). Then non-uniform changes are applied to the grid during n_{max} time steps to end up with the uniform grid, identical to the initial one. From a mathematical point of view for all $1 \leq i \leq n_x$, $1 \leq j \leq n_y$ and $0 \leq n \leq n_{max}$ by

$$x_{i,j}^n = (1 - \alpha_n)\xi_{i,j} + \alpha_n\xi_{i,j}^3, \quad (8.1)$$

$$y_{i,j}^n = (1 - \alpha_n)\eta_{i,j} + \alpha_n\eta_{i,j}^2, \quad (8.2)$$

where

$$\xi_{i,j} = \frac{i-1}{n_x-1}, \quad \eta_{i,j} = \frac{j-1}{n_y-1}, \quad \alpha_n = \frac{1}{2} \sin\left(\frac{4\pi n}{n_{max}}\right). \quad (8.3)$$

Note that if $n = 0$ or $n = n_{max}$ then $\alpha_n = 0$ therefore $x_{i,j}^0 = x_{i,j}^{n_{max}} = \xi_{i,j}$ and $y_{i,j}^0 = y_{i,j}^{n_{max}} = \eta_{i,j}$ (see Fig.15 for examples of grids).

The profiles used are of three kinds: (i) a smooth profile (sinus), (ii) a shock profile, where a step function defines the density, velocity and energy profiles, (iii) an exponential shock profile where the post shock density/energy regions are defined with an exponential function.

Clearly if the remapping was an exact process then the profiles at $t = 0$ and $t = t_{n_{max}}$ would be identical. However some diffusion is added by the remapping during the successive n_{max} steps. Comparing the initial and final profiles give a measure of how well/bad the remapping process performs, independently of the rest of the code.

The computation is performed with several meshes: 15×15 , 33×33 , 65×65 , 128×128 , 257×257 and the errors in L_1, L_2, L_∞ norms, namely $\bar{\rho}_1, \bar{\rho}_2, \bar{\rho}_\infty$ are computed for these meshes as:

$$\bar{\rho}_1 = \sum_c |\rho(c) - \rho^{ex}(x_c, y_c)| V(c), \quad (8.4)$$

$$\bar{\rho}_2 = \sum_c |\rho(c) - \rho^{ex}(x_c, y_c)|^2 V(c), \quad (8.5)$$

$$\bar{\rho}_\infty = \max_c |\rho(c) - \rho^{ex}(x_c, y_c)|, \quad (8.6)$$

moreover the maximum norm of density is computed as

$$\|\rho\|_\infty = \max_c |\rho(c)|. \quad (8.7)$$

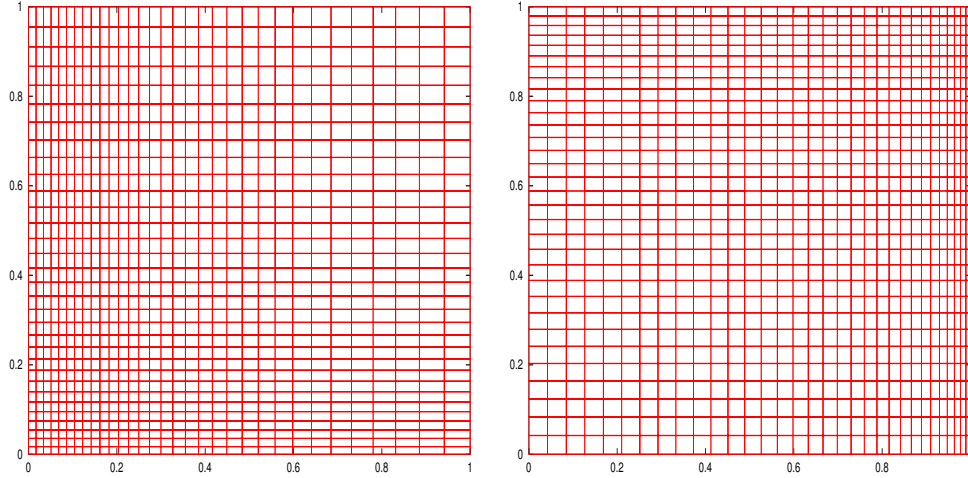


Figure 15: Tensor product grids — $n_x \times n_y = 33 \times 33$ — Grids at cycle 30 (left) and 200 (right).

Mesh	$\bar{\rho}_1$	Ratio	$\bar{\rho}_2$	Ratio	$\bar{\rho}_\infty$	Ratio	$\ \rho\ _\infty$	Ratio
15×15	$2.826E - 2$	—	$1.234E - 3$	—	$1.216E - 1$	—	1.8948	—
33×33	$4.951E - 3$	5.71	$6.398E - 5$	19.28	$3.132E - 2$	3.88	1.9696	3.46
65×65	$1.234E - 3$	4.01	$7.395E - 6$	8.65	$1.721E - 2$	1.82	1.9897	2.95
128×128	$3.126E - 4$	3.95	$9.408E - 7$	7.86	$9.162E - 3$	1.88	1.9965	2.94
257×257	$7.799E - 5$	4.01	$1.123E - 7$	8.38	$4.746E - 3$	1.93	1.9988	2.92

Table 1: Pure remapping problem for the sinus profile (density) — Error in L_1, L_2, L_∞ and the ratio between two consecutive errors.

Smooth profile. On $\Omega = [0, 1] \times [0, 1]$ a fluid is initiated with

$$\rho^{ex}(x, y) = 1 + \sin(2\pi x) \sin(2\pi y), \quad (8.8)$$

$$\mathbf{u}^{ex}(x, y) = (0, 0), \quad (8.9)$$

$$\varepsilon^{ex}(x, y) = 0. \quad (8.10)$$

In table 1 are gathered the errors for the variable density. In Fig.16 are presented the density after 320 (33×33 grid) and 1280 (128×128 grid) remapping steps.

Shock profile. On $\Omega = [0, 1] \times [0, 1]$ a fluid is initiated with

$$\rho^{ex}(x, y) = \begin{cases} 1 & \text{if } x \leq 0.5 \\ 0.125 & \text{else} \end{cases} \quad (8.11)$$

$$\mathbf{u}^{ex}(x, y) = \begin{cases} (1, 0) & \text{if } x \leq 0.5 \\ (0, 0) & \text{else} \end{cases} \quad (8.12)$$

$$\varepsilon^{ex}(x, y) = \begin{cases} 2.5 & \text{if } x \leq 0.5 \\ 2.0 & \text{else} \end{cases} \quad (8.13)$$

In table 2 are gathered the errors for the density, velocity and specific internal energy in The errors for the

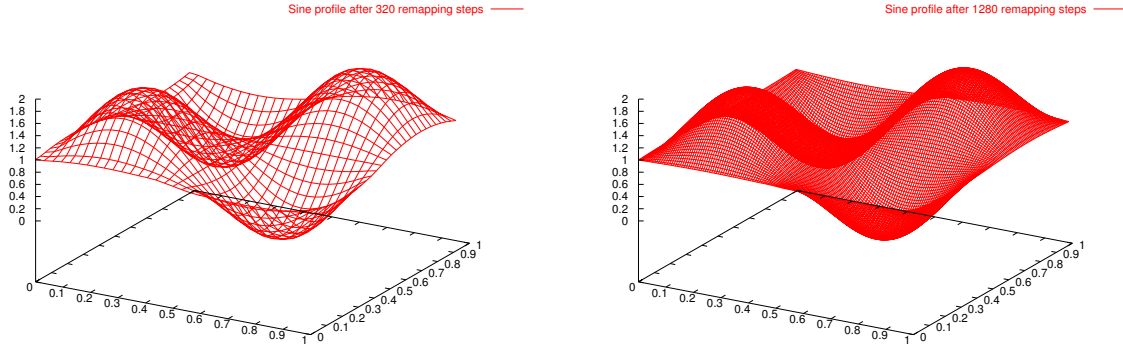


Figure 16: Sinus profile after 320 remapping steps on a 33×33 mesh and 1280 remapping steps on a 128×128 mesh.

Mesh	$\bar{\rho}_1$	Ratio	$\bar{\rho}_2$	Ratio	$\bar{\rho}_\infty$	Ratio
15×15	$4.170E - 2$	—	$9.638E - 3$	—	$2.711E - 1$	—
33×33	$2.245E - 2$	1.86	$5.482E - 3$	1.76	$2.976E - 1$	0.91
65×65	$1.333E - 2$	1.68	$3.360E - 3$	1.63	$3.177E - 1$	0.94
128×128	$7.999E - 3$	1.67	$2.074E - 3$	1.62	$3.555E - 1$	0.89
257×257	$4.714E - 3$	1.70	$1.233E - 3$	1.68	$3.250E - 1$	1.01
Mesh	\bar{u}_1	Ratio	\bar{u}_2	Ratio	\bar{u}_∞	Ratio
15×15	$5.207E - 2$	—	$4.179E - 2$	—	$9.116E - 1$	—
33×33	$2.550E - 2$	2.04	$1.960E - 2$	2.13	$8.985E - 1$	1.01
65×65	$1.436E - 2$	1.77	$1.069E - 2$	1.83	$8.902E - 1$	1.00
128×128	$7.636E - 3$	1.88	$5.072E - 3$	2.11	$8.544E - 1$	1.04
257×257	$4.600E - 3$	1.66	$3.259E - 3$	1.56	$8.804E - 1$	0.97
Mesh	$\bar{\epsilon}_1$	Ratio	$\bar{\epsilon}_2$	Ratio	$\bar{\epsilon}_\infty$	Ratio
15×15	$9.974E - 2$	—	$4.052E - 2$	—	1.900	—
33×33	$5.986E - 2$	1.67	$2.433E - 2$	1.67	1.900	1.00
65×65	$4.018E - 2$	1.49	$1.645E - 2$	1.47	1.900	1.00
128×128	$2.378E - 2$	1.69	$9.405E - 3$	1.75	1.900	1.00
257×257	$1.353E - 2$	1.76	$4.736E - 3$	1.99	1.899	1.00

Table 2: Pure remapping problem for the shock profile — Error in L_1, L_2, L_∞ and the ratio between two consecutive errors.

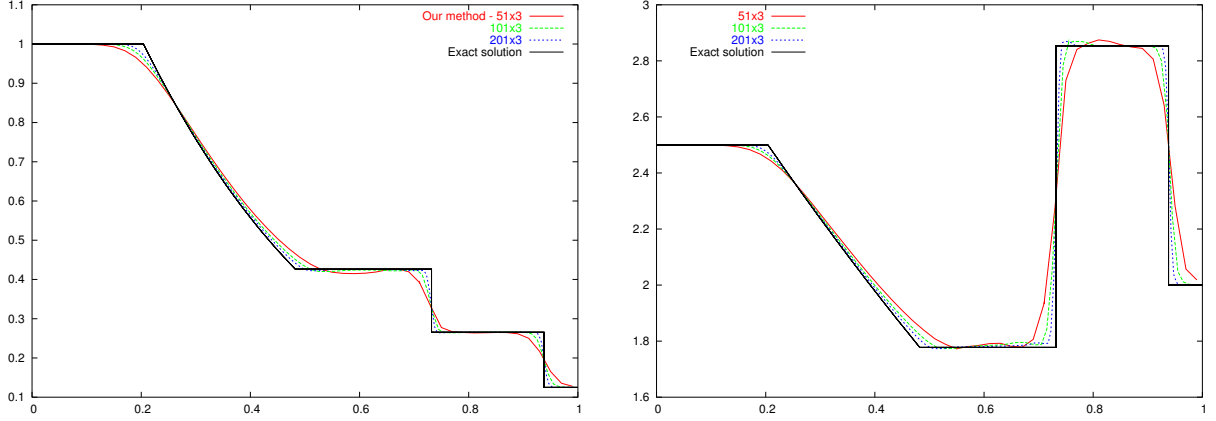


Figure 17: Convergence for Sod problem — Lagrange+Remap regime — Density and specific internal energy at $t = 0.25$ for $n_x = 50, 100, 200$.

velocity are computed as

$$\bar{u}_1 = \sum_n |u(n) - u^{ex}(x_n, y_n)| m(n), \quad (8.14)$$

$$\bar{u}_2 = \sum_n |u(n) - u^{ex}(x_n, y_n)|^2 m(n), \quad (8.15)$$

$$\bar{u}_\infty = \max_n |u(n) - u^{ex}(x_n, y_n)|, \quad (8.16)$$

and for the specific internal energy

$$\bar{\varepsilon}_1 = \sum_c |\varepsilon(c) - \varepsilon^{ex}(x_c, y_c)| V(c), \quad (8.17)$$

$$\bar{\varepsilon}_2 = \sum_c |\varepsilon(c) - \varepsilon^{ex}(x_c, y_c)|^2 V(c), \quad (8.18)$$

$$\bar{\varepsilon}_\infty = \max_c |\varepsilon(c) - \varepsilon^{ex}(x_c, y_c)|. \quad (8.19)$$

8.2 Simplified hydrodynamics context

Most of the validation test cases are gathered into [28] where the remapping component has been tested as a stand-alone process and embedded into ALE INC.

The following tests are mostly the ones used to validate the Lagrangian scheme (see section 4) but the code has been ran in its Euler as Lagrange+Remap regime. By doing that we cancel the effect of the rezoning process, only the scheme and the remapping component are tested. Most of the tests are 1D Riemann problems (Sod, Le Blanc etc.) or known 1D flows (blastwave, rarefaction, expansion in vacuum etc) where the grid is composed of squares aligned with the waves.

ALE INC. has been compared with classical Lagrange+Remap schemes (from R.Pember (LLNL, Livermore), Benson (UCSD, San Diego)) with success on these classical test problems.

1D Sod Riemann problem. In Fig. 17 we present the exact solution and the density for resolutions $n_x = 50, 100, 200$, and $n_y = 3$.

1D LeBlanc Riemann problem. In Fig. 18 we present the exact solution and the specific internal energy for the LeBlanc shock tube problem for 360, 720, 1440 grid resolution in x direction.

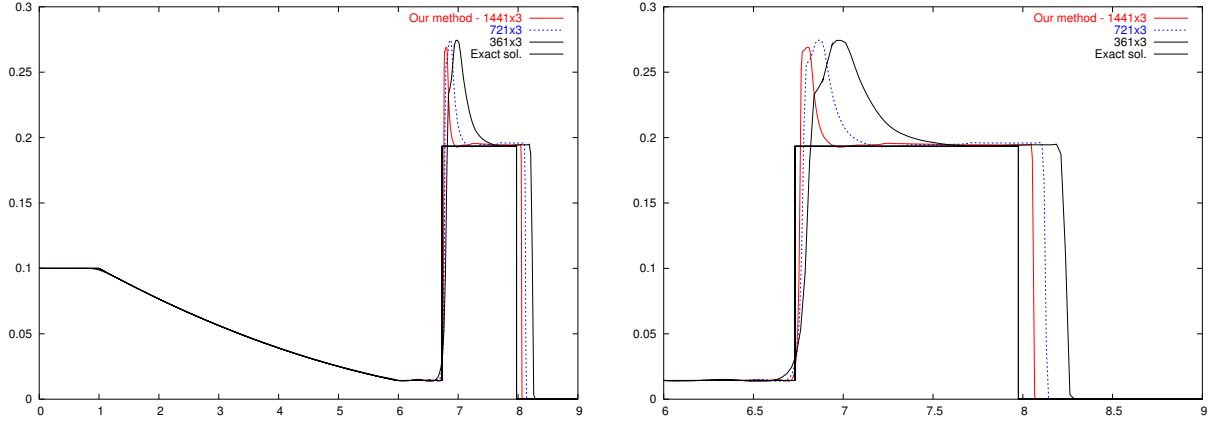


Figure 18: Convergence for Le Blanc problem — Lagrange+Remap regime — Specific internal energy at $t = 6.0$, $n_x = 360, 720, 1440$: entire computational domain (left), zoom (right).

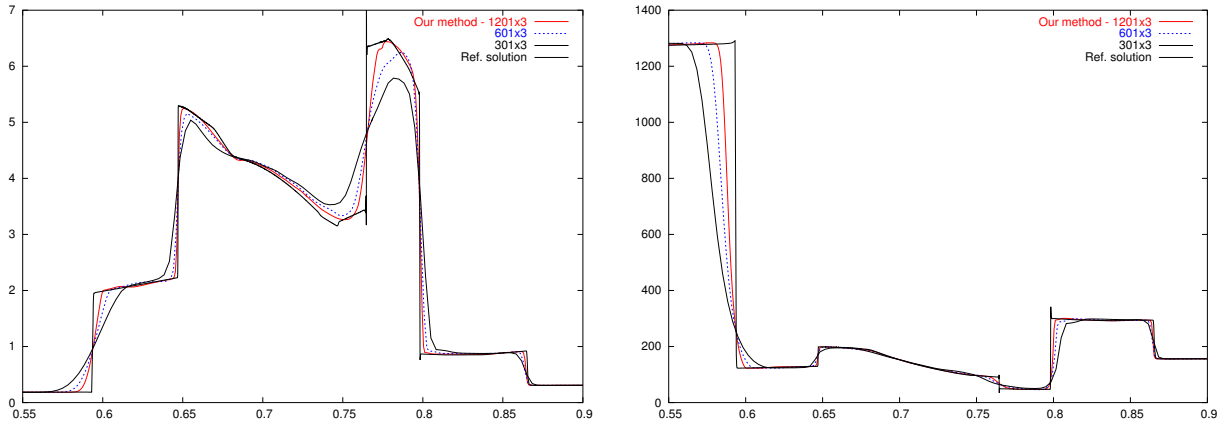


Figure 19: Convergence for Woodward-Colella Blast Wave Problem at $t = 0.038$, $n_x = 300, 600, 1200$ — Lagrange+Remap regime — Left: density (zoom) — Right: specific internal energy (zoom).

1D Colella-Woodward blastwave. In Fig. 19 we graphically demonstrate the convergence rate for the Colella-Woodward blastwave Problem on the set of meshes with resolutions $n_x = 300, 600, 1200$. We present numerical results both for density and specific internal energy. Because there is no analytical solution for this problem we do not present a table with convergence rates.

9 Cylindrical geometry

10 ALE INC(ubator)

In this section we simply present the behavior of ALE INC as a simulation code for well-known compressible fluid flows in 2D situations. the point is not to describe all these test cases but rather to present how the code behaves on these well-known problems.

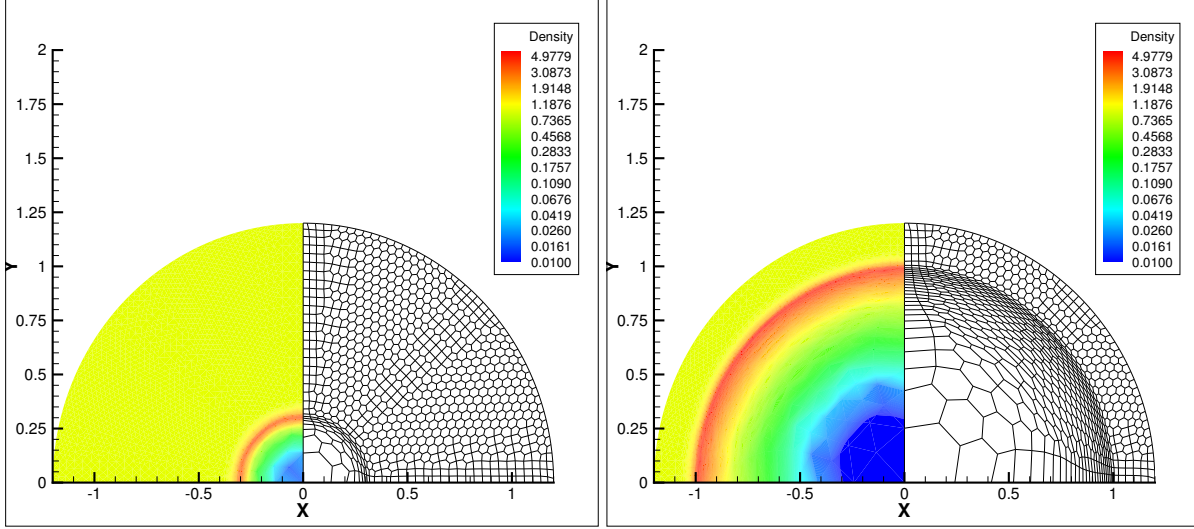


Figure 20: Sedov problem for a polygonal mesh — ALE-20 regime — Left: $t = 0.1$ mesh and density field — Right: $t = 1.0$ mesh and density field.

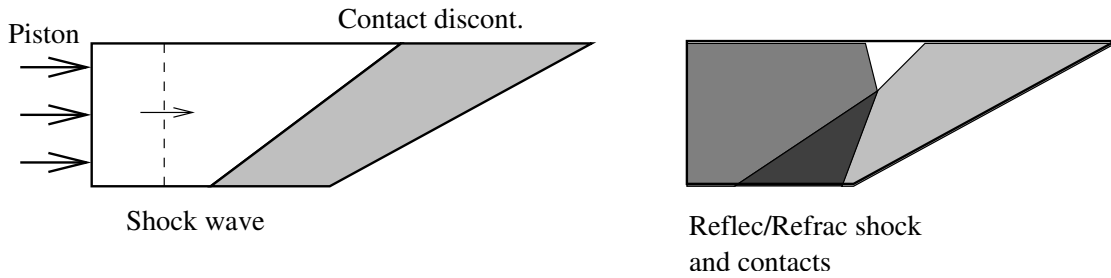


Figure 21: Dukowicz problem — ALE-20 regime — Left: Initial shock wave — Right: after multiple refraction/reflection.

Sedov problem. In this paragraph the code simulates the Sedov problem in ALE-20 regime for the same polygonal mesh as in section ??.

Dukowicz problem. The dukowicz problem describes the interaction of a shock wave sent by a piston and an oblique contact discontinuity (see Fig.21). In Fig.22 is presented the density field at $t = 1.3$ for a polygonal mesh with approximatively 60 point in x -direction and 40 in the y -direction. The ALE-20 regime is used.

Triple point problem. This problem is briefly described in Fig.23 where a shock wave is sent from below (middle density field). It lately impacts two contiguous regions, one with a high density (left), one with a low density (right). At the triple point a vortex develops, away from the triple point a simple 1D Riemann problem occurs in the y -direction. Fig.24 presents the density field and the mesh at $t = 0.7$ for an initial perfect quadrangular mesh with 81×81 points. The ALE-20 regime is used.

Rayleigh-Taylor instability. A gravity field is applied in the vertical (y) direction. Moreover the initial interface between a heavy fluid (top) and a light fluid (bottom) is perturbed like a sinus wave then a Rayleigh-Taylor instability develops as described in Fig.25. In Fig.26 is presented the density field at $t = 8.5$

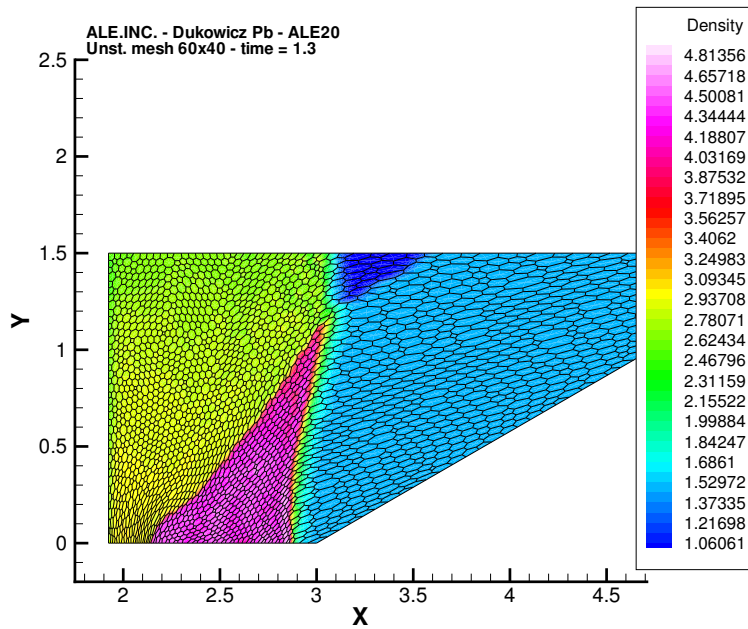


Figure 22: Dukowicz problem on unstructured mesh — ALE-20 regime — Density at $t = 1.3$.

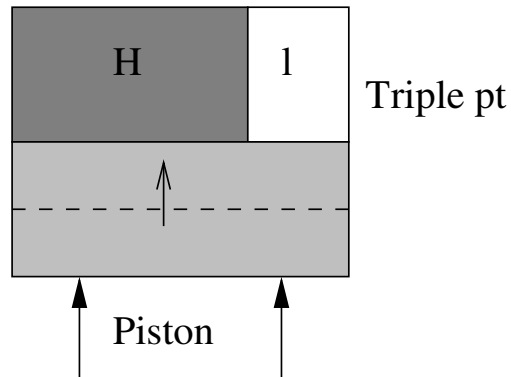


Figure 23: Triple point problem — A shock wave (dashed line) is sent from below across a middle density field (light gray). It impacts two contiguous regions, one with a high density (H to the left, dark gray), one with a low density (l to the right, white). At the triple point a vortex develops, away from the triple point a simple 1D Riemann problem occurs in the vertical direction.

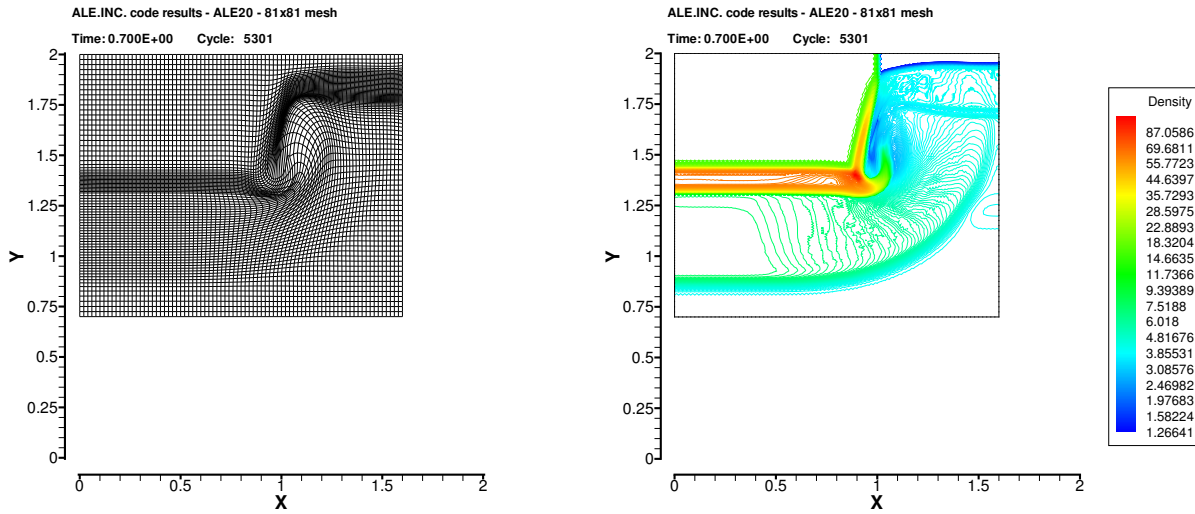


Figure 24: Triple point problem for an initial perfect quadrangular mesh with 81×81 points — Left: final mesh — Right: final density field.

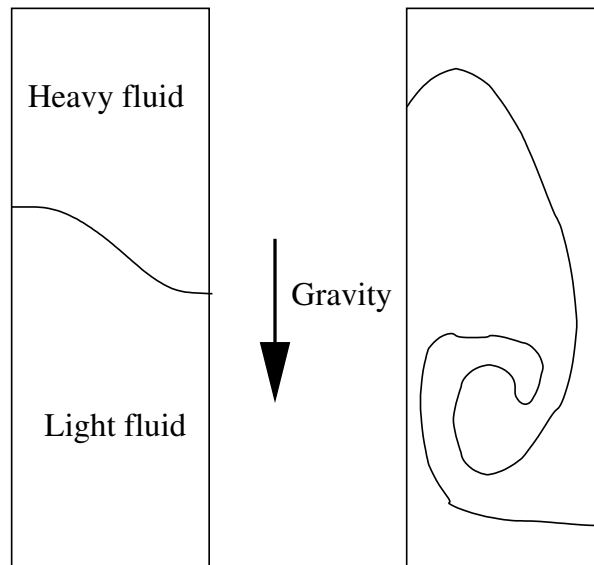


Figure 25: Rayleigh-Taylor instability — Left: Two fluids (heavy and light) are separated by a non planar interface under gravity field — Right: a Rayleigh-Taylor instability develops.

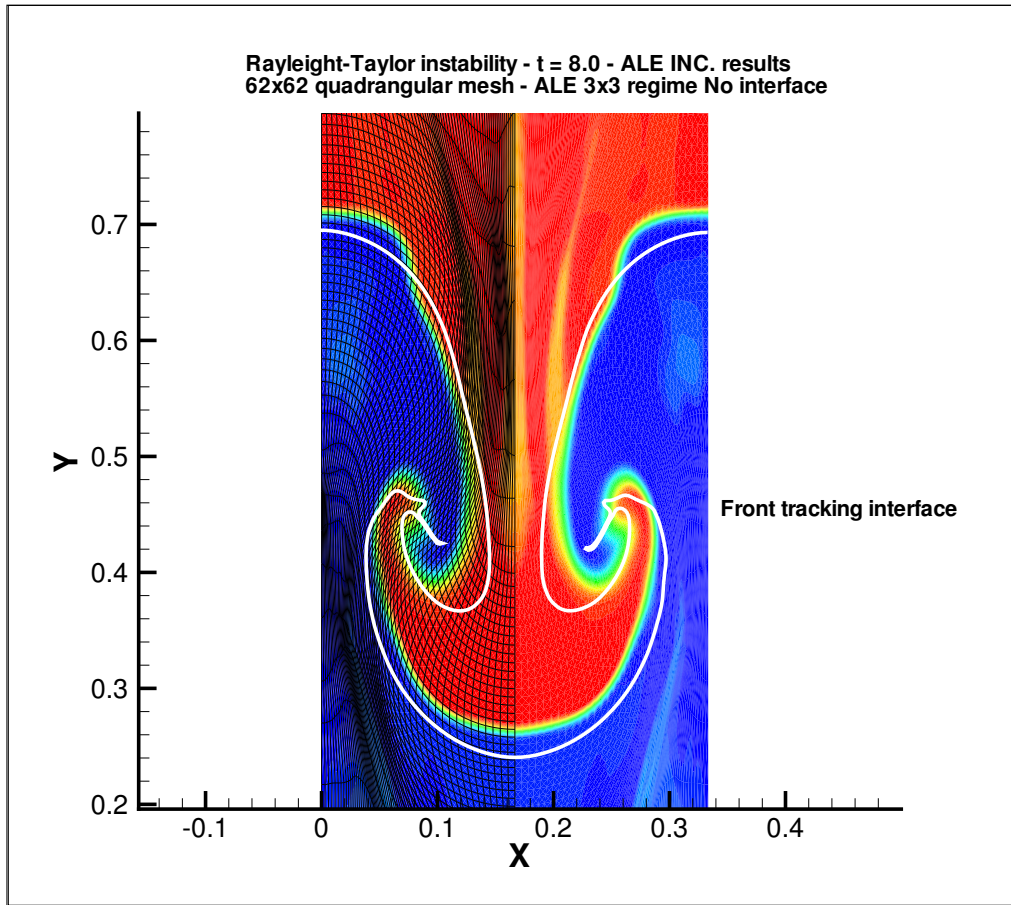


Figure 26: Rayleigh-Taylor instability at $t = 8.5$ — ALE- 3×3 regime — Density and mesh compared with the solution given by a Front tracking method (white line) — Initial mesh is a quadrangular 62×62 mesh.

11 Conclusion

References

- [1] A.A. Amsden, H.M. Ruppel and C.W. Hirt, *SALE: A Simplified ALE Computer Program for Fluid Flow at All Speeds*, Los Alamos National Laboratory Report LA-8095 (1980).
- [2] T. J. Barth, *Numerical Methods for Gasdynamics Systems on Unstructured Grids*, in Lecture Notes in Computational Science and engineering, "An Introduction to Recent Developments in Theory and Numerics for Conservation Laws, Proceedings of the International School on Theory and Numerics for Conservation Laws, Freiburg/Littenweiler, October, 20-24, 1997, D. Kroner, M. Ohlberger, C. Rohde (Eds.) Springer, Berlin, 1997, pp. 195–285.
- [3] D. J. Benson, *An Efficient, Accurate, Simple ALE Method for Nonlinear Finite Element Programs*, Computer Methods in Applied Mechanics and Engineering, **72** (1989), pp. 305–350.
- [4] D. J. Benson, *Computational Methods in Lagrangian and Eulerian Hydrocodes*, Computer Methods in Applied Mechanics and Engineering, **99** (1992), pp. 235-394.
- [5] D. J. Benson, "Momentum Advection on a Staggered Grid," J. Comp. Phys. **100** pp. 143-162 (1992).
- [6] D. E. Burton, "Multidimensional Discretization of Conservation Laws for Unstructured Polyhedral Grids", Report UCRL-JC-118306, Lawrence Livermore National Laboratory, 1994.
- [7] D. E. Burton, "Consistent Finite-Volume Discretization of Hydrodynamics Conservation Laws for Unstructured Grids" Report UCRL-JC-118788, Lawrence Livermore National Laboratory.
- [8] J. Campbell and M. Shashkov, *A Compatible Lagrangian Hydrodynamics Algorithm for Unstructured Grids*, Selcuk Journal of Applied Mathematics, **4** (2003) pp. 53–70; report version can be found at (<http://cnls.lanl.gov/shashkov>),
- [9] J. Campbell, M. Shashkov, *A tensor artificial viscosity using a mimetic finite difference algorithm*, Journal of Computational Physics, **172** (2001), pp. 739–765.
- [10] E. J. Caramana and M. J. Shashkov, *Elimination of Artificial Grid Distortion and Hourglass-Type Motions by means of Lagrangian Subzonal Masses and Pressures*, Journal of Computational Physics, **142** (1998), p. 521 .
- [11] E. J. Caramana, M. J. Shashkov and P. P. Whalen, *Formulations of Artificial Viscosity for Multi-Dimensional Shock Wave Computations*, Journal of Computational Physics, **144** (1998), p. 70.
- [12] E. J. Caramana, D. E. Burton, M. J. Shashkov and P. P. Whalen *The Construction of Compatible Hydrodynamics Algorithms Utilizing Conservation of Total Energy*, Journal of Computational Physics, **146** (1998), p. 227.
- [13] R.B. Demuth, L.G. Margolin, B.D. Nichols, T. F. Adams and B.W. Smith, "SHALE : a Computer Program for Solid Dynamics", Report Los Alamos National Laboratory Report LA-10236, 1985.
- [14] C. W. Hirt, A. A. Amsden and J. Cook, "An Arbitrary Lagrangian-Eulerian Computing Method for All Flow Speeds", J. Comp. Phys. **14** pp. 227–253 (1974), and reprinted in **135** pp. 203–216 (1997).
- [15] C.W. Hirt and A.A. Amsden, "YAQUI: An Arbitrary Lagrangian-Eulerian Computer Program for Fluid Flow at All Speeds," Los Alamos Scientific Laboratory Report LA-5100 (1973).
- [16] D.S. Kershaw, M.K. Prasad, M.J. Shaw, and J.L. Milovich, *3D Unstructured Mesh ALE Hydrodynamics with the Upwind Discontinuous Finite Element Method*, Computer Methods in Applied Mechanics and Engineering, **158** (1998), pp. 81–116.
- [17] P. Kjellgren and J.Hyvarien. *An Arbitrary Lagrangian-Eulerian Finite Element Method*, Computational Mechanics, **21** (1998), pp. 81–90.

- [18] P. Knupp, L.G. Margolin, M. Shashkov, *Reference Jacobian Optimization-Based Rezone Strategies for Arbitrary Lagrangian-Eulerian Methods*, Journal of Computational Physics, **176** (2002), pp. 93–12.
- [19] M. Kucharik, M. Shashkov, and B. Wendroff, *An Efficient Linearity-and Bound-Preserving Remapping Method*, Journal of Computational Physics, **188** (2003), pp. 462–471.
- [20] L.G. Margolin and C.W. Beason, *Remapping on the Staggered Mesh*, Report UCRL-99682 of Lawrence Livermore National Laboratory (1988).
- [21] L.G. Margolin, *Introduction to "An Arbitrary Lagrangian-Eulerian Computing Method for All Flow Speeds*, J. Comp. Phys. **135** pp. 198–202 (1997).
- [22] L. G. Margolin and M. Shashkov. *Remapping, Recovery and Repair on Staggered Grid*, LA-UR-03-2230, Computer Methods in Applied Mechanics and Engineering, to appear.
- [23] J. M. McGlaun, S. L. Thompson, and M. G. Elrick, *CTH: A Three Dimensional Shock Wave Physics Code*, Int. J. Impact Engng., **10** (1990), pp. 351–360.
- [24] R. B. Pember and R. W. Anderson, *A Comparison of Staggered-Mesh Lagrange Plus Remap and Cell-Centered Direct Eulerian Godunov Schemes for Eulerian Shock Hydrodynamics*, Preprint UCRL-JC-139820, Lawrence Livermore National Laboratory, 2000.
- [25] J. S. Peery and D. E. Carroll, *Multi-Material ALE Methods in Unstructured Grids*, Computer Methods in Applied Mechanics and Engineering, **187**, (2000), pp. 591–619.
- [26] M. Shashkov and P. Knupp, "Optimization-Based Reference-Matrix Rezone Strategies for Arbitrary Lagrangian-Eulerian Methods on Unstructured Grids", Selcuk J. Appl. Math. 3(1) pp. 81–99 (2002).
- [27] P.Vachal, R.Garimella, M. J. Shashkov, R.Loubere, *Untangling of meshes in ALE simulations*, Proceedings of 7th US Nat. Congress on Computational Mechanics, Albuquerque, July 2003.
- [28] R.Loubere, M.Staley, B.Wendroff, *The repair paradigm: New Algorithms and Applications to compressible flow*, Report Los Alamos National Laboratory Report LA-UR-04-0795, 2004, submitted to J. Comp. Phys.
- [29] R.Loubere, M. J. Shashkov, *A Subcell Remapping Method on Staggered Polygonal Grids for Arbitrary-Lagrangian-Eulerian Methods*, Report Los Alamos National Laboratory Report LA-UR-04-6692, 2004, submitted to J. Comp. Phys.
- [30] P. Vachal, R. Garimella, and M. Shashkov, *Untangling of 2D meshes in ALE simulations*, Journal of Computational Physics, **196** (2004), pp. 627–644.
- [31] M. Ainsworth and J. T. Oden, *A Posteriori Error Estimation in Finite Element Analysis*, A Wiley-Interscience Publication, John Wiley & Sons, Inc., 2000.
- [32] M. J. Baines *Moving Finite Elements*, Oxford Science Publications, Clarendon Press, Oxford, 1994.
- [33] J.U. Brackbill and J.S. Saltzman, *Adaptive Zoning for Singular Problems in Two Dimensions*, Journal of Computational Physics, **46** (1982), pp. 342–368.
- [34] D. E. Carroll, Sandia National Laboratories, NM, (private communication, 2000).
- [35] A. Charakhch'yan and S. Ivanenko, *A variational form of the Winslow grid generator*, J. Comput. Phys., **136** (1997), pp. 385–398.
- [36] J. Donea, S. Giuliani, and J. P. Halleux, *An Arbitrary Lagrangian-Eulerian Finite Element Method for Transient Dynamic Fluid-Structure Interactions*, Computer Methods in Applied Mechanics and Engineering, **33** (1982), pp. 689–723.
- [37] J.K. Dukowicz, *A Simplified Adaptive Mesh Technique Derived from the Moving Finite Element Method*, Journal of Computational Physics, **56** (1984), pp. 324–342.

- [38] J.K. Dukowicz and J.W. Kodis, *Accurate Conservative Remapping (Rezoning) for Arbitrary Lagrangian-Eulerian Computations*, SIAM J. Stat. Comput., **8** (1987), pp. 305–321.
- [39] J.K. Dukowicz, M.C. Cline and F.L. Addressio, *A General Topology Godunov Method*, Journal of Computational Physics, **82** (1989), pp. 29–63.
- [40] L. Freitag and P. Knupp, *Tetrahedral Element Shape Optimization via the Jacobian Determinant and Condition Number*, Proceedings of the 8th Intl. Meshing Roundtable, S. Lake Tahoe CA, 1999, pp. 247-258,
- [41] S. Giuliani, *An Algorithm for Continuous Rezoning of the Hydrodynamic Grid in Arbitrary Lagrangian-Eulerian Computer Codes*, Nuclear Engineering and Design, **72** (1982), pp. 205–212.
- [42] J. Glimm, J. W. Grove, X.-L. Li, K.-M. Shyue, Q. Zhang, and Y. Zeng. *Three dimensional front tracking*, SIAM J. Sci. Comp., **19** (1998), pp. 703–727.
- [43] J. Glimm, J. Grove, X.-L. Li, W. Oh, and D. H. Sharp. *A critical analysis of Rayleigh-Taylor growth rates*, J. Comp. Phys., 2000, To appear, SUNY Preprint SUNYSB 00-19; LANL LA-UR 99-5582.
- [44] C.W. Hirt, A.A. Amsden and J.L. Cook, *An Arbitrary Lagrangian-Eulerian Computing Method for All Flow Speeds*, Journal of Computational Physics, **14** (1974), pp. 227–253, reprinted in **135** (1997), pp. 203–216.
- [45] D.S. Kershaw, M.K. Prasad, M.J. Shaw, and J.L. Milovich, *3D Unstructured Mesh ALE Hydrodynamics with the Upwind Discontinuous Finite Element Method*, Computer Methods in Applied Mechanics and Engineering, **158** (1998), pp. 81–116.
- [46] P. Kjellgren and J.Hyvarien. *An Arbitrary Lagrangian-Eulerian Finite Element Method*, Computational Mechanics, **21** (1998), pp. 81–90.
- [47] P. Knupp, *Mesh generation using vector-fields*, J.Comput.Phys., **119**, pp142-148, 1995.
- [48] P. Knupp, *Jacobian-weighted Elliptic Grid Generation*, SIAM J. Sci. Comput., Vol. 17, No. 6, pp1475-1490, 1996.
- [49] P.Knupp, *Achieving finite element mesh quality via optimization of the Jacobian matrix norm and associated quantities. Part I - A framework for surface mesh optimization*, Int. J. Numer. Meth. Engng., **48** (2000), pp. 401–420.
- [50] P.Knupp, *Achieving finite element mesh quality via optimization of the Jacobian matrix norm and associated quantities. Part II - A framework for volume mesh optimization and the condition number of the Jacobian matrix*, Int. J. Numer. Meth. Engng., **48** (2000), pp. 1165-1185.
- [51] P. Knupp, *Matrix Norms and the Condition Number - A general framework to improve mesh quality via node-movement*, Proceedings of the 8th Intl. Meshing Roundtable, S. Lake Tahoe CA, 1999, pp. 13- 22.
- [52] P. Knupp and N. Robidoux, *A Framework for Variational Grid Generation: Conditioning the Jacobian Matrix with Matrix Norms*, SIAM J. Sci. Comput., **21** (2000), pp. 2029–2047.
- [53] H. J. Kull, *Theory of the Rayleigh-Taylor Instability*, Physics Reports, **206** (1991), pp. 197–325.
- [54] V.D. Liseikin, *Grid Generation Methods*, Springer, 1999, pp. 91–93.
- [55] R. Lohner and C. Yang, *Improved ALE Mesh Velocities for Moving Bodies*, Communications in Numerical Methods in Engineering, **12** (1996), pp. 599–608.
- [56] L. G. Margolin and J. J. Pyin, *A Method of Treating Hourglass Patterns*, in Proc., Numerical Methods in Laminar and Turbulent Flow, edited by C. T. Taylor and N. M. Hafey (1987), p. 149.

- [57] N. Mikhailova, V.Tishkin, N.Turina, and A.Favorskii, and M. Shashkov *Numerical modeling of two-dimensional gasdynamics flows on a variable-structure mesh*, - U.S.S.R. Comput. Maths. Math. Phys. **26** (1986), pp. 74–84.
- [58] J. Nocedal and S. J. Wright, *Numerical Optimization*, Springer Series in Operations Research, Springer-Verlag New York Inc., 1999.
- [59] D. Kroner and M. Ohlberger, *A Posteriori Error Estimates for Upwind Finite Volume Schemes for Nonlinear Conservation Laws in Multi Dimensions*, Math. of Comp., **69** (1999), pp. 25–39.
- [60] J. S. Peery and D. E. Carroll, *Multi-Material ALE Methods in Unstructured Grids*, Computer Methods in Applied Mechanics and Engineering, **187**, (2000), pp. 591–619.
- [61] M. Shashkov, *Conservative Finite-Difference Methods on General Grids*, CRC Press, Boca Raton, 1995.
- [62] A. I. Shestakov, J. A. Harte, and D. S. Kershaw. *Solution of the Diffusion Equation by the Finite Elements in Lagrangian Hydrodynamic Codes*, Journal of Computational Physics, **76**, pp. 385-413, (1988).
- [63] C. Stoker, C. Gay, F. Bay, and J.-L. Chenot, *A Velocity Approach for the ALE-method applied for 2D and 3D Problems*, Simulation of Material Processing: Theory, Methods and Applications, Huetink and Baaijens (eds)., 1998 Balkema, Rotterdam.
- [64] A. N. Tikhonov and A. A. Samarskii, *Equations of Mathematical Physics*, A Pergamon Press Book, The Macmillan Company, New York, 1963.
- [65] J.G. Tinoco-Ruiz, *Funcionales Discretos para la Generacion de Mallas Suaves y Convexas sobre Regiones Planas Irregulares*, Ph.D. Thesis, CIMAT, Guanajuato, Mexico, 1997.
- [66] A. Winslow, *Numerical solution of the quasilinear Poisson equations in a nonuniform triangle mesh*, J. Comput. Phys., **1**, (1966) pp. 149-172.